

We wish to sincerely thank both reviewers for careful reading of the manuscript and their thoughtful comments and criticism that have helped us improve its quality. We have addressed all comments raised by the reviewers to the best of our knowledge, and hope the revised version could better guide the readers through the methods we used and the mechanisms we proposed.

Below, we copy the reviewers' comments in bold and blue color, followed by the point-to-point reply. With the response we also send the revised manuscript and supplementary figures.

## Response to Reviewer#1

### 1 Scientific Comments

#### **Objection#1: A poor model**

**No model is ever perfect, and the authors do acknowledge that. However, I am concerned that the excessive semi-annual cycle, the absence of a combination tone, and the very strong link to the annual cycle (see Objection 2 below) really limit the generalizability and usefulness of these simulations.**

We acknowledge that our model may ignore some important mechanisms that is associated with ENSO dynamics as recent studies reveal. However, there is still an improvement of the model from the latest study of this topic (Timmermann et al., 2007), by which we show a possible mechanism of complete difference. Single model study is indeed not enough to fully understand this difficult question (ENSO sensitivity to the orbital modulation). We hope our study can inspire more related studies using other models.

The semi-annual cycle is caused by the shift in phase of the annual cycle, a point we did not notice before (and thought it to be a bias!) and failed to demonstrate in the previous manuscript. Actually, the tropical Pacific annual cycle in the accelerated simulation is quite reasonable: it agrees with the non-accelerated TRACE-ORB in amplitude (Fig. 1g), and agrees with GFDL model snapshots (Erb et al., 2015) in phase. The phase modulation by precession has been studied in another paper by us (Lu and Liu, 2017), in which more analysis is presented.

We have revised Sec 6.1 to comprehensively discuss the model performance in the tropical Pacific and the acceleration effect.

The model performance issue is also noticed by reviewer#2 (comment 4), and a similar reply can be found.

#### **Objection#2: Frequency entrainment**

**The authors also seem to believe in the frequency entrainment mechanism as an explanation for virtually everything. Although it does seem to explain the orbital response of most PMIP3 models, it does not apply to all GCMs, especially a more realistic one [An, SI. & Choi, J. Clim Dyn (2013) 40: 663. doi:10.1007/s00382-012-1403-3]. More importantly, it was recently shown to be incompatible with observations over the Holocene [Emile-Geay et al., (2015), doi:10.1038/ngeo2608]. The authors cite the latter paper but seem to completely discount its critical conclusion, and how this conclusion undermines most of their reasoning. Let me, therefore, rephrase it: in a model where the annual cycle runs the show, one will infer relations to forcings that are overly centered on the annual cycle. This would be actively misleading, perhaps worse than no model at all. I urge the authors to seriously consider the implications of frequency entrainment being an unphysical aspect of CCSM3, perhaps by targeted experiments with other community models like GFDL's CM2.1, which does not exhibit this behavior (and presumably reacts differently to orbital forcing). It is no longer good enough to assume that frequency entrainment explains everything.**

The Nonlinear mechanisms controlling ENSO variance that we already know are actually not many. For example, there are the frequency entrainment and the combination mode. We have tested frequency entrainment because the orbital modulation of annual cycle in CCSM3 shows robust precession signal (e.g. Fig. 1g), so it is necessary to see the relationship between annual cycle and ENSO.

The frequency entrainment mechanism is robust in CCSM3 model, for example, under millennial fresh water discharge (Timmermann, et al., 2007; Liu et al., 2014); it also explains the CO<sub>2</sub> and ice-sheet forcing on ENSO (Liu et al., 2014; Lu et al., 2016).

The orbital forcing of ENSO, on the contrary, is quite different. We quantitatively show that the nonlinear terms contribute almost negligibly to the SST tendency (see reply to comment 5 of reviewer#2). Emile-Geay et al. (2015) do show inconsistency between high resolution reconstruction (in-phase change of interannual and seasonal variability of the past 10 kyr) and PMIP3 simulations (out-of-phase change of interannual and seasonal variability in mid-Holocene and PI simulations). And our orbital forcing simulation, accelerated and unaccelerated (ORB, TRACE-ORB and TRACE), agrees with the proxy on ENSO-AC relationship.

On the other hand, our results suggest that the combination mode does not exist in our model. And we speculate it is due to the biennial ENSO bias.

### **Objection#3: Problematic acceleration**

**Central to the long time span claimed in the title (300,000 years) is the hundred-fold acceleration technique used by the authors. Just because it's been done 15 years ago, doesn't mean it's a good thing to do today. To their credit, the authors do a good job of using the TRACE simulation to evaluate the consequences of the acceleration. However, they fail to adequately emphasize in their conclusions how seriously this alters the model's response compared to the non-accelerated case, which in my view completely undermines the rest of their conclusions. To wit: the response to orbital variations takes place during 200 years, not 20,000. This is barely sufficient for ventilation to takes place in the lower thermocline, and seriously compromises any claim made about the quantitative importance of the thermocline feedback, to take one example. The authors partly concede this, but in my opinion this needs to be the main topic of the paper: acceleration is a bad idea, and completely distorts the physics of the response. There is still value in the results presented in this article, but only from the strict perspective of paleo modeling techniques.**

**The applicability of CCSM3 results to the real world is questionable, but still of interest. The applicability of accelerated CCSM3 results to the real world is non-existent.**

**In summary, major revisions are needed to bring the title and abstract of this work in line with what can be reliably concluded from these simulations.**

We acknowledge that the acceleration can be problematic, but the result still provides an example to study ENSO sensitivity under 'pseudo' modulation of insolation. The revised manuscript shows more quantified analysis on the effect of acceleration in Sec 6.1.

Please see more details in reply to comment 2 of reviewer#2.

### **2 Editorial Comments**

#### **• The English is remarkably poor.**

Thanks for the advice and the example from the reviewer. The revised manuscript will be carefully proof-read.

#### **• The Thomas et al 2006 reference lists the paper as 'in review'... 10 years ago. What is the current status of this article?**

The paper has been published on GRL in 2017. The reference list is updated.

## Response to Reviewer#2

### Main comments:

**1. The scope of the study is of course important as there is still a large uncertainty about the impact of external forcing (both past and future) on ENSO properties. The authors propose an ambitious modelling study with potentially interesting results. This said the current manuscript has some severe issues that need addressing to fully realise this potential.**

We thank all the comments and critics from the reviewer. Please see our reply to the specific issues below.

**2. The first major issue the impact of acceleration. The authors do point out this may lead to issue at sub-surface but do not provide any quantification of this effect. The comparison with the un-accelerated TRACE runs remains qualitative and unconvincing. In particular Fig. 1f questions the relevance of this comparison and no proper statistical analysis is provided. This is all the more problematic as the dominant mechanisms invoked for ENSO change involve the sub-surface ocean.**

We agree with the reviewer that more statistical analysis is needed to show the impact of acceleration.

1. We add some discussion associated with the the Appendix (Effect of Accelerated Forcing in a One-Dimensional Diffusive Ocean) of Timm and Timmermann (2007), which also applies to this study. It gives us a framework of the magnitude of acceleration effect in the deep ocean using a simple diffusive model. Furthermore, the phase lag estimated from this simple model is consistent with that calculated by comparing ORB and TRACE-ORB (e.g. Fig. 1d). The former estimates a phase lag of 2000 accelerated years at 200m depth, while the latter shows a longer lag of about 5000 accelerated years at the thermocline depth when including oceanic subduction process.

2. We would like to stress that the annual cycle (Fig. 1g), both in amplitude and phase, is quantitatively consistent for accelerated and non-accelerated simulations. It provides an evidence for the surface (or the mixed layer) equilibrium of mean climate even in the tropical Pacific using acceleration. In addition, ENSO dynamics is associated with ocean dynamics no deeper than thermocline depth, so it is still interesting to study its change in the accelerated simulation.

3. Even if the acceleration could pose serious problems to understand ENSO change under orbital time scale modulation, to see results from the ENSO response from 'pseudo' 200-yr precession-magnitude and 400-yr obliquity-magnitude insolation modulation can still improve our understanding of climate evolution and ENSO sensitivity.

We will quantitatively show these points in the revised discussion sections 6.1 and 6.3.

We address the concern for robustness of ENSO precession signal (Fig. 1f) in the next comment.

**3. The second major issue is the lack of proper quantification and significance testing of the results. In many cases, the analysis is weakened by this lack of quantification. Most prominently, the significance of the ENSO change signal in Fig. 1f is not clear and is not tested against a proper null hypothesis (no forcing) – this issue is briefly touched upon in the discussion but not properly addressed (qualitative analysis of Fig. S6 is not sufficient), putting the rest of the manuscript in jeopardy. Appropriate statistics (error bars/correlations/significance testing, etc.) are needed in all figures to ensure that the analysis only concentrates on actual signals and not noise.**

We calculate the power spectrum for the time series of ENSO amplitude, and its ~21ka frequency peak passes 95% significance level. It suggests the primary change in ENSO amplitude is due to the precessional forcing. See revised discussion section 6.3.

In addition, as we argued in the manuscript, the relative change (about half of +15%) of ENSO amplitude in the mid-Holocene (~6ka) to pre-industrial is in the within the range of PMIP snapshots as that of TRACE experiment.

We believe these two evidences are enough to support our argument against the no forcing null hypothesis.

For other issues associated with proper quantification or significance test, please also refer to more details in reply to minor comments (e.g., # 5, 20).

**4. The third major issue is the tropical Pacific and ENSO performance in CCSM3 – more details should be given on how well the model is doing (mean annual cycle, seasonal phase locking of ENSO, etc. . .), including the use of the BJ index to analyse it, as for example discussed in Kim and Jin (2010) (e.g. their Fig. 9). Also the implications of the 2 years pendulum behaviour are not fully explored. Currently there are only a few lines on this key issue.**

Thanks for pointing it out. Indeed, more details of the model performance in the tropical Pacific should be added in the manuscript, especially for tropical annual cycle and ENSO variance phase locking (Sec 6.1).

In fact, these issues are discussed in another paper (Lu and Liu, 2017). We gain more confidence as our accelerated simulation results are in qualitative agreement with other studies. For example, the phase of seasonal cycle (Erb et al., 2015) and ENSO variance phase locking (Karamperidou et al., 2015).

The discussion about Fig. 9 in Kim and Jin (2010) mainly focuses on the relative contribution of each BJ term on the total BJ index, which we have already done when discussing our Fig. 4b.

Please also see reply to the reviewer#1 (comment 1).

It seems the quasi-biannual ENSO bias is robust in both accelerated and unaccelerated CCSM3 simulations. This bias can have two potential impacts: first it is speculated that the combination mode vanished because of this bias; it somehow shortens the typical ENSO time scale and can increase the number of ENSO events during a certain period which also increases the sample size to calculate the correlation of evolution of BJ index and ENSO (when analyzing the linear mechanism).

There are also minor comments related to this issue (e.g., #16,17 and 47), please also see the reply to them.

**5. The fourth major issue has to do with the BJ index itself and its underlying linear assumptions. After some initial success for CMIP3 and a couple of other cases, the BJ index has since not been successful in evaluating model ENSO errors (for instance, not working for CMIP5). Graham et al. (2014) attributed this lack of skill precisely to the linear assumptions made in the deriving the BJ index. Using the full on-line heat budget in a model they showed that the BJ index misrepresents the true magnitude of the ENSO ocean feedbacks. It seems that as models improve and exhibit a similar degree of non-linearity as observations, linear analysis frameworks as proposed here became no longer reliable guides for model analysis. Whether this applies to CCSM3 or not has to be investigated. A related issue is the impact of acceleration on the nonlinear behaviour of ENSO in this model. For these reasons (and the lack of proper model evaluation – see point above) section 4.1 too quickly dismisses the role of nonlinearities (either in ENSO or in its interactions with the annual cycle).**

Thanks for the suggestion. The Graham et al. (2014) paper shows a practical way to estimate the uncertainty in BJ calculation. Following their method, we use heat budget to check the contribution from the linear terms as well as the nonlinear terms. It is found in orbital modulation of CCSM3 simulation the nonlinear behavior of ENSO is negligible (Fig. S3).

We also add the error bars to the BJ terms, which estimate the uncertainty from the regression (Fig. S4).

The discussion of validity of BJ index is added in P9L23-31.

Minor comment #25 also points out this question.

**6. Finally there are a number of conjectures (no evidence provided) and vague terms (“slow”, “dominated”, “closely tracks”, “follows more closely”, “less robust”, “can be largely explained”, “weaker”, “resemble closely”, “enhanced”, “tend to be closer”, “al- most identical”, “fairly consistent”, “good agreement”, “higher”, “smaller”, “seems quite robust”, “pronounced”, etc.) that weaken the manuscript and should be either removed or properly defined/quantified. Also a few phrases need to proof read as the English is not correct.**

We thank the reviewer for careful reading of the manuscript. The conjectures and vague terms are modified to our best knowledge. For example, see reply to comments #12,16,20,21,24,25,27,35,38,39,41,43,45 and 48.

The revised manuscript will be carefully proof-read.

**Other comments:**

**7. The abstract is vague and its language needs tightening.**

It is revised.

**8. P.2 L. 6: more recent ref needed.**

We add IPCC AR5 (Christensen et al., 2013), from which the conclusion is similar.

**9. L. 6-10: much too quick of an intro for this important topic. and 10. L. 11, what do the authors mean by “slow” ENSO evolution ? An why focus on this ? What do paleo observations provide us to compare with ?**

This topic is explained in more details. See P2L9-18.

The ‘slow’ means orbital time scale, or longer. It is interesting to study the ENSO sensitivity to orbital modulation because current proxy data (especially since the mid-Holocene) can constrain the model uncertainty of simulated ENSO variance. Also because the current PMIP 6ka simulations is mainly about to study orbital modulation, which can be compared with our results.

We will put this topic and more description about the paleo ENSO observations in the introduction.

**11. L. 17-19: please provide references for this statement.**

It is a conclusion from Liu et al. (2014).

**12. L. 30: I read carefully the Liu et al. study and was not convinced by the BJ analysis (mostly because of the points highlighted above).**

The method of BJ is tested. See more details in reply to comment 5.

**13. P.3, l. 1-7 : there are many ENSO mechanisms – why focus on these only ?**

We were trying to give a review of previous orbital forcing mechanism of ENSO variance, those studies listed were interested to us, which includes both linear and nonlinear mechanisms.

**14. L.8 : please detail the “different processes”.**

The processes are added. Please see P3L18-20.

**15. L. 23-24: please provide reference(s) and mechanism(s).**

Yes. It is Chiang et al. (2009).

**16. P.4 l. 8-11: much too quick - see issue 4 above.**

**and 17. L. 15-16: please explain.**

We move all model performance in accelerated simulation discussion to Sections 6.1 and 6.3.

In short, since even the 100-fold accelerated orbital time scales, say, 200-yr for precession and 400-yr for obliquity is far longer than that of typical tropical surface climate processes, e.g., the annual cycle and ENSO. This point is tested quantitatively in the discussion sections 6.1 and 6.3.

**18. L. 30-31: how is this done w.r.t the land-sea mask and heat and fresh water local/global conservation at the air-sea and land-sea interfaces?**

The sea level is changed only with context of the land-sea distribution (e.g., during the glacial period the Bering Strait is closed which implies the lowering of sea level), so the fresh water conservation is not strictly valid, but such a small amount should not affect low-latitude climate too much.

**19. L. 32-33: this is cryptic for non-experts. Please explain.**

Yes, they are explained in P5L12-16.

**20. P.5 l. 22-25: how significant are these changes w.r.t to a null hypothesis ?**

Please see reply to comment 3.

**21. L. 31: please explain this conjecture.**

we will remove this conjecture.

**22. P.6 l. 16: please clarify.**

Done (P7L1).

**23. L. 20: which non-linear mechanisms are we talking about here ?**

We mainly focus on the frequency entrainment mechanism, which is proposed in a previous accelerated orbital forcing simulation (Timmermann et al., 2007). The combination mode is also tested later, but it turns out not a robust feature in our model.

**24. P. 7, l.1-26: this is much too quick (see point 4 above). ECHO-G is notorious for having quite degraded climatology and balance of processes in the eastern Pacific cold tongue (due to crude vertical mixing scheme). Proper comparison is required to have confidence in the points (too quickly) made in this section.**

Since the ECHO-G simulation is the only previous modelling study on this topic, it is necessary to compare its wavelet spectrum (main feature of frequency entrainment, and the killer figure of their paper) with our results. We would argue that a qualitative comparison of the power spectrum is reassuring that the frequency entrainment cannot explain the change of ENSO variance in our simulation, in addition to the plots of evolution of ENSO and annual cycle (Fig. 1f,g).

The significance level of precession signal in ENSO variance, on the other hand, is tested in reply to comment 3.

**25. P. 8 l. 24-28: what is the impact of these ? Did you compare to actual tendencies such as in Graham et al. (2014) ? More is needed to go beyond the current “cuisine” feel when reading this.**

Thanks for pointing it out. The impact is that the absolute value of BJ index is increased (now close to 0), but not its trend on the orbital time scale.

BJ index itself is tested as seen in reply to comment 5.

**26. P. 9 l.2 why is the relative BJ index change the right measure?**

The absolute value of BJ index can be different due to different methods of estimation, for example, the choice of region (e.g., equatorial eastern Pacific or Nino 3.4), the processing method (e.g. band-pass filter). So its relative change can be more meaningful, and reveals the influence of external forcing.

**27. P. 9 l. 4-15: please quantify all qualitative and vague terms.**

**and 28. L. 4-10: is a correlation of 0.4 large enough to infer a causality link? Again here proper significance testing is missing. Please use the 21k simulation to show that the “acceleration can make the forcing signal less robust”. And what would be the mechanisms? This key section is quite unclear and not convincing.**

More details of the quantification of acceleration effect can be found in Sec 6.1.

Both the evolution of ENSO variability and its linear growth rate (BJ) are predominately modulated by the precessional forcing, as confirmed by analysis on the frequency domain (e.g., Fig. S1a and Fig.S8a). In accelerated simulation, the correlation between them is 0.4, and is higher when the precession modulation is more pronounced (e.g. 250~100 ka BP).

By comparing the accelerated and unaccelerated simulations, it can be concluded that the acceleration can dampen and delay the precession signal in the ocean. A comprehensive discussion on the acceleration effect can be found in Sec 6.1.

**29. L. 24-31: this conjecture is not really convincing.**

This argument is now supported by more quantified explanation (P10L23-L30).

**30. L. 31 – p.10. l. 2: then what is the point of analysing slow ENSO variations if a basic mechanism affecting the thermocline slope is not correct?**

Indeed the precession signal is dampened and delayed in the deeper ocean, but the BJ index still shows pronounced 21 ka cycles (confirmed by the coherence analysis). A more detailed analysis on each feedback of the BJ index suggest the thermocline feedback ( $w_{\text{bar}}dzT'$ ) does show a larger uncertainty than the most important Ekman upwelling feedback ( $w' dzT_{\text{bar}}$ ).

**31. L. 10-14: yes, I agree with this caveat.**

Unfortunately, the reason for this caveat is not clear to us.

**32. L. 18: WWBs are not a “remote” forcing.**

OK. We change it to ‘stochastic’ forcing.

**33. L. 24-25: how reliable is this approach ? Have you tested it for a period when both frequencies are available in the output ? Otherwise, this section is not convincing.**

As the equations after the argument show, the approach should be reliable. Unfortunately, due to the limited computational resources, we did not save the output higher than monthly resolution.

**34. P. 11 l. 9: please clarify.**

Done

**35. P. 12 l. 11-22: please quantify all qualitative and vague terms.**

Done. (P13L12-25). Additionally, we also add power spectrum analysis for ENSO in ORB+GHG and ORB+GHG+ICE.

**36. L. 28-34 – p. 13 l.4: I am probably missing something as a I thought increased GHGs were enhancing ENSO amplitude?**

The CCSM3 model shows increased GHGs could weaken ENSO. We copy the description of the nonlinear mechanism below:

*The increased GHGs concentration leads to an asymmetric annual mean warming (a stronger warming north of the equator) in the tropical Pacific (Figure not shown), which enhances the equatorial asymmetry and in turn the annual cycle (Timmermann et al., 2004). The enhanced annual cycle then weakens ENSO through frequency entrainment (Liu, 2002). The ice sheet change, also predominant in the 100-kyr cycle, forces an in-phase change of annual cycle intensity and an out-of-phase change of ENSO intensity.*

**37. P. 13 l. 8-12: too quick – please explain.**

Done (P14L10-18).

**38. L. 12-19: conjecture – please show it or remove point.**

We have reorganized this part (P14L9-30).

First the quantified results are shown: in ORB+GHG, the correlation between ENSO strength and BJ is increased, and BJ has pronounced frequency peak at ~21 ka and a secondary peak at ~ 100 ka (not significant). It somehow implies the possible relation between the ENSO linear growth rate and the GHG forcing.

Second, we speculate that it can be explained by a previous proposed mechanism (Meehl et al., 2006, and they used the same CCSM3 model), by which the CO<sub>2</sub> warming at the sea surface leads to a more diffusive equatorial thermocline and weakened ENSO. The hypothesis is hard to be quantified because we only have available data for the upper ocean (above ~50m).

**39. L. 25-32: because of the lack of proper significance testing and of issue with non linear mechanisms, it is hard to follow this discussion.**

The discussion of the effect of different forcing combination can only be quantified if more sensitivity experiments are done, e.g., single forcing 300 ka accelerated simulation. Since our purpose is only to remind the readers of this issue in our simulation, we move it to the discussion Sec 6.2.

**40. P.14,l. 6: why?**

Please see reply to comment 10. It is previously defined as ‘slow’ evolution of ENSO variance.

**41. L. 6-32: please quantify all qualitative and vague terms.**

**and 42. L. 17-19: by which measure(s) are the accelerated and TRACE simulations “fairly consistent”?**

Done. And the ‘fairly consistent’ amplitude and phase are quantified. See the revised Sec 6.1.

**43. Section 6.2: please quantify all qualitative and vague terms.**

Done.

**44. L. 31 – p. 16 l.2: isn’t this a circular argument? If not, please clarify.**

It is not, because both tropical mean climate (annual cycle) and climate variability (ENSO) are quantitatively consistent for accelerated and unaccelerated simulations during the last 21 ka.

**45. Section 6.3: see point 4 above**

Power spectrum discussion is added.

**46. L. 10-13: a low correlation can also be due to physics! Why should one expect 100% correlation if the sampling is right?**

In the revised manuscript we quantify the effect of acceleration below the surface ocean, and we hope these analyses (Secs. 6.1 and 6.2) more evidently support our argument.

**47. L. 13-16: indeed and please expand on this important caveat.**

Yes. The biennial ENSO could increase the number of ENSO events (sample size). We add more details of ENSO phase locking when replying to comment 4.

**48. Conclusion: please quantify all qualitative and vague terms.**

Done.

**49. P. 17 l. 12-16: this is an unsupported conjecture, not a conclusion**

See reply to comment 36, 38 and Lu et al., 2016.

**Reference**

Please see those in the manuscript.

# Evolution and forcing mechanisms of ENSO over the last 300,000 years in CCSM3

Zhengyao Lu<sup>1</sup>, Zhengyu Liu<sup>2,1</sup>, Guangshan Chen<sup>2</sup>, Jian Guan<sup>1</sup>

<sup>1</sup>Lab. Climate, Ocean and Atmosphere Studies, School of Physics, Peking Univ., Beijing, 100871, P. R. China

5 <sup>2</sup>Dept. Atmospheric and Oceanic Sciences & Nelson Center for Climatic Research, Univ. of Wisconsin-Madison, Madison, WI53706, USA

*Correspondence to:* Zhengyao Lu (zlu@pku.edu.cn; luzhengyao88@gmail.com)

**Abstract.** The responses of El Niño-Southern Oscillation (ENSO) and the equatorial Pacific annual cycle to external forcing changes are studied in three 3,000-year-long NCAR-CCSM3 model simulations. The simulations represent the period from 10 300 thousand years before present (ka BP) to present day. The first idealized simulation is forced only with accelerated orbital variations, and the rest are conducted more realistically by sequentially adding on the time-varying boundary conditions of greenhouse gases (GHGs) and continental ice sheets.

It is found that the orbital forcing dominates slow (orbital time scales) ENSO evolution, while the effects of GHGs and ice- 15 sheet forcing tend to compensate each other. ENSO variability and annual cycle amplitude change in-phase and both have pronounced precessional cycles (~21,000 years) modified by variations of eccentricity. Precession modulated ENSO intensity is dominated linearly by the change of the coupled ocean-atmosphere instability, notably the Ekman upwelling feedback; and it is also affected modestly during ENSO intrinsic developing season by the influences of the short-scale stochastic weather noise outside the equatorial eastern Pacific. The acceleration technique is found to dampen and delay the 20 precessional signal below the surface ocean (associated with ENSO intensity), by directly comparing the accelerated simulation with the non-accelerated counterpart.

In glacial-interglacial cycles, additionally, the weakening/strengthening of ENSO owing to a more concentrated/depleted GHGs level leaves little net signal as compensated by the effect coherent change of decaying/expanding ice sheets. They 25 influence the ENSO variability through changes in annual cycle amplitude via a common nonlinear frequency entrainment mechanism.

## 1 Introduction

ENSO is the largest year-to-year climate variability and has a huge societal and economic impact on a great human population. Despite significant progress towards understanding its changing mechanisms (e.g. Bjerknes, 1969; Philander, 1990; Neelin et al., 1998; Suarez and Schopf, 1988; Batisti and Hirst, 1989; Jin, 1997a,b; Philander and Fedorov, 2003; Yu and Kao, 2007; Kao and Yu, 2009; Wang et al., 2012), predictions of future climate projections for ENSO variability are still far from satisfactory (e.g. Meehl et al., 2007; Christensen et al., 2013). In the future, the features of ENSO, e.g. its intensity, could be changed, as implied by adequate proxy reconstructions for at least the last 10,000 years (e.g. Tudhope et al., 2001; Moy et al., 2002; Riedinger et al., 2002; Conroy et al., 2008; Koutavas et al., 2012; Cobb et al., 2013; Carre et al., 2014; Ford et al., 2015; Emile-Geay et al., 2015) attributed to the variations of multiple external forcings. Specifically, the change of ENSO variance during the Holocene, especially since the mid-Holocene (~6ka BP), can provide a perfect case to understand its sensitivity to orbital modulation because the insolation was remarkably different while the greenhouse gases (GHGs) concentration and ice sheet coverage were relatively similar compared to the pre-industrial period. In addition, relatively abundant proxy reconstructions, either from earlier lake sediments (e.g. Moy et al., 2002; Conroy et al., 2008) or more recent high-resolution data of oxygen isotope (see a summary of these data in Emile-Geay et al., 2015) suggest ENSO was intensified since the mid-Holocene, which potentially constrains the model uncertainties of simulated future ENSO variance. Prior to the Holocene, there are limited available proxy reconstructions (e.g., Tudhope et al., 2001; Koutavas et al., 2012). They somehow show ENSO were active as early as 150 ka BP, despite large changes in the external forcings including insolation as well as greenhouse gases and ice-sheets and the consequent completely different mean climate. In short, it is important to study the change of ENSO dynamics of the past, e.g., its sensitivity to the orbital modulation, to gain some clues for the future.

One more specific question is: what is the forcing mechanism for the slow (orbital time scale) evolution of ENSO during the glacial-interglacial cycles (e.g. late-Pleistocene)? To address this question, in a previous study we have examined a set of transient Coupled General Circulation Model (CGCM) simulations forced by realistic external forcing in combination and individually for the last 21,000 years (hereafter TRACE, Liu et al., 2014). The simulated ENSO gradually intensifies during the Holocene (by about 15%), primarily due to and in phase with the precessional forcing, suggesting the orbital forcing as the primary forcing for its overall slow evolution. Moreover, the ENSO response to slow modulation of GHGs and ice-sheet forcings seem not to play a significant role, partly because of a compensation effect between the two. In addition, during early deglaciation, ENSO amplitude shows large modulations on millennial time scales forced by the melt water fluxes.

Still, the ENSO evolution in the past and its governing mechanisms are only beginning to be understood, which provides a motivation for this study. First, we want to explore the ENSO response to the orbital forcing that consists of full cycles of eccentricity (~100 ka), obliquity (~41 ka) and precession (~21 ka), including extreme precessional forcings modulated by

larger eccentricity than during the last deglaciation. Second, we want to evaluate the contribution from other forcings relative to the orbital forcing, notably from the GHGs and continental ice sheet, both being dominated by a saw-tooth shaped quasi-100 ka oscillations (Petit et al., 1999).

5 In particular, we want to further understand the mechanism of ENSO response to orbital forcing. Earlier studies speculated the monsoon forcing (Liu et al., 2000) or local change of seasonal coupled instability (Clement et al., 1999) as the major mechanism of ENSO response to orbital forcing. In TRACE, Liu et al. (2014) highlighted the role of the linear coupled instability, or ocean-atmosphere feedbacks, especially the Ekman upwelling feedback, as the dominant mechanism that modulates the ENSO amplitude in response to precessional forcing. The Ekman upwelling feedback is modulated by the equatorial stratification through the South Pacific water mass subducting in austral winter in response to the precessional forcing. In contrast, however, in a study of a transient climate simulation of the last 142,000 years forced by the orbital forcing (accelerated by 100-time), Timmermann et al. (2007) suggested that ENSO amplitude is modulated by the interaction between ENSO and the seasonal cycle via the nonlinear mechanism of frequency entrainment, with a stronger annual cycle leading to a weaker ENSO (Liu, 2002). In a study of mid-Holocene ENSO response, Chiang et al. (2009) suggested that ENSO is reduced by a weaker extratropical atmospheric stochastic forcing communicating equatorward through a pronounced reduction in the Pacific Meridional Mode (PMM) activity. A recent study by Roberts et al. (2014) quantitatively showed that the changed mean state during the early/mid-Holocene is responsible for stabilized ENSO (and reduced ENSO variance) compared with modern day in simulations of two CGCMs, however, by completely different processes (in CSM mean cooling of the SST, reduced atmospheric heating anomalies and smaller wind stress anomalies, or in HadCM3 a combination of a weaker thermocline and weakened horizontal surface currents) that weakens the Bjerknes feedback. All these discrepancies could be caused by different models, different experimental settings such as the acceleration technique, or even different interpretations using the very same simulation output (Roberts et al., 2014) therefore call for more thorough studies.

25 Here, we extend our ENSO study to the late-Pleistocene by analyzing a set of simulations of the climate evolution of the last 300,000 years (or 300 ka), as a follow-up study of ENSO in the last 21,000 years in TRACE, using the same climate model (NCAR-CCSM3). Three experiments are performed, which are forced by the orbital forcing (ORB), orbital and GHGs forcing (ORB+GHG), and the additional continental ice sheet (ORB+GHG+ICE). We only focus on the slow evolution of ENSO on the orbital time scale and thus have excluded the meltwater fluxes forcing. All model forcings are accelerated by 100 times as in the orbital-alone simulation of Timmermann et al. (2007). Therefore, our simulations here can be compared with Timmermann et al (2007) on the effect of different models, and with TRACE on the effect of forcing acceleration. Our results show that ENSO amplitude varies predominantly in phase with the precessional forcing during the last 300,000 years, due to the changes in ocean-atmosphere coupled instability; ENSO also weakens due to increased GHGs and a strengthens

due to ice-sheet retreat, all being qualitatively consistent with TRACE. Other extratropical influences such as stochastic forcing and the PMM may also contribute to the evolution of ENSO variability (Chiang et al., 2009).

The paper is organized as follows. In Section 2 the model and simulations are described. In Section 3 we explore basic ENSO features in the orbital forcing simulation. In Section 4 we propose that ENSO variability is controlled predominantly by the linear mechanism of coupled instability, although it may also be influenced by stochastic forcing outside the eastern equatorial Pacific. In Section 5 we discuss ENSO responses to GHGs and ice-sheet forcing. Finally, in Section 6 and 7 we provide a discussion and a summary of the main results.

## 2 Model and experiments settings

Our model is the National Center for Atmospheric Research Community Climate System Model, version 3 (NCAR-CCSM3). The model has a low resolution (Yeager et al., 2006; Otto-Bliesner et al., 2006). The atmospheric model is the Community Atmospheric Model 3 (CAM3), with a  $\sim 3.75^\circ$  latitude-longitude resolution (T31) and 26 hybrid coordinate levels in the vertical. The land model also has a T31 resolution, and each grid box includes a hierarchy of land units (glaciers, lakes, wetlands, urban areas, and vegetated regions can be specified), soil columns, and plant types. The ocean model is the NCAR implementation of the Parallel Ocean Program (POP), with a  $\sim 3.6^\circ$  longitudinal resolution, a variable latitudinal resolution ( $\sim 0.9^\circ$  near the equator, gx3v5) and 25 vertical z coordinate levels. The sea ice model is the NCAR Community Sea Ice Model (CSIM), a dynamic-thermodynamic model that includes a subgrid-scale ice thickness distribution. The resolution of CSIM is identical to that of POP. It should be noted here that the model is not subject to annual mean flux-correction on both the heat and freshwater fluxes as in Timmermann et al. (2007).

20

In order to test the global climatic impact of orbital forcing, the orbital simulation of 3,000-year-long (hereafter, ORB) was performed in which the orbital forcing is applied with an acceleration factor of 100 in time, starting from 300 ka BP and ending in present day (0 ka BP). The tropical climate and surface ocean are expected to be in quasi-equilibrium with the acceleration technique (Timmermann et al., 2007). There is a comprehensive discussion on acceleration effect and model performance in the tropical Pacific in Sec 6.1. The simulation was initialized with pre-industrial conditions and the GHGs concentration and ice-sheet volume were prescribed as the pre-industrial level (Sec 6.2).

Our main focus will be on the mechanism of ENSO response in ORB. Since tropical climate and ENSO variability can also be changed by other forcings during the late-Pleistocene, notably GHGs, ice sheet orography and albedo (Timmermann et al. 2004; An et al. 2004), we performed two additional simulations. One used the accelerated orbital forcing as well as accelerated GHGs forcing (both with an acceleration factor of 100) of the last 300 ka but with prescribed pre-industrial ice-sheets (hereafter, ORB+GHG); the other further included accelerated variation of continental ice sheets as the lower

boundary condition to the atmosphere (ORB+GHG+ICE). The time resolution of equivalent CO<sub>2</sub> level (CO<sub>2</sub> and CH<sub>4</sub>) was associated with the Antarctica ice core reconstruction (Petit et al., 1999; Augustin et al., 2004). The time resolution of the varying ice sheets of the last 21 ka is the same as the ICE-5G (VM2) reconstruction (Peltier, 2004), and the ice-sheet coverage was interpolated based on the global sea level reconstruction (Waelbroeck et al., 2002) back to 300 ka BP (Thomas et al., 2017, also see their Method for more details of the model settings). In ORB+GHG+ICE which includes three kinds of external forcings, for example, the orbital parameters and the GHGs were advanced by 100 years at the end of each model year, while the continental ice sheet volume (and land-sea distribution associated with the sea level change) was changed at steps of an equivalent 40-m sea level rise or fall to reconfigure and restart the model.

10 During the post-process of model data, in order to remove the artificial phase shifts on the climatic responses in these 300 ka paleoclimate simulations, the output (monthly) was converted to the “fixed-angular” calendar from the “fixed-day” calendar based on Chen et al. (2010). The “fixed-day” calendar defines months following the present-day calendar for any period of the past with the vernal equinox (VE) fixed at March 21 noon or with the autumnal equinox (AE) fixed at September 23 noon, while the “fixed-angular” calendar is defined so that each month begins and ends at the same celestial longitude as present-day for any period of the past with the VE designated as 0° celestial longitude. Although equivalent for the present, in the past due to change in orbital parameters, the two calendars are different in the length of the seasons. However, it is found that the simulated mean climate or climate variability (e.g. ENSO strength and tropical Pacific annual cycle amplitude) does not change much after the calendar correction (Figure not shown).

### 3 Basic features of ENSO and annual cycle in ORB

20 In this section we describe the evolution of tropical mean climate and climate variability in ORB. Fig. 1 (black curves) shows the evolution of orbital parameters (Berger and Loutre, 1991) in the simulation, and it consists of obliquity cycles with ~41 ka periodicity (Fig. 1a) and precessional cycles with ~21 ka periodicity modulated by ~100 ka period of eccentricity (Fig. 1b). The obliquity is responsible for the existence of seasons on earth while its variation mainly influences the annual cycle at high latitudes. The precession, when associated with the changes in eccentricity, dominates the variations in insolation at low and mid latitudes. It affects the position of seasons related to perihelion and that effect increases across all the latitudes during the period of larger eccentricity (e.g. ~220 ka BP and ~120 ka BP); it hardly matters if eccentricity is near zero and the earth orbit is close to a circle.

The simulated tropical mean climate manifests remarkable orbital forcing signals. Over the eastern equatorial Pacific (EEP), 30 the annual mean SST closely tracks the obliquity (Fig. 1a,c), while a larger/smaller obliquity (larger/smaller tilt and less/more annual mean insolation over the tropics) leads to lower/higher SST. Under the sea surface, the evolution of the subsurface sea temperature in the EEP (Fig. 1d), unlike that of the SST, follows the precessional cycles with a ~5ka lag, due

to the subduction process (a more detailed discussion about the process can be found in Secs. 4.2 and 6.1). The cross-equatorial EEP meridional SST gradient also has precessional cycles (Fig. 1e), a situation consistent with Timmermann et al., (2007).

5 The most striking feature of the ENSO evolution is that the ENSO amplitude is modulated predominantly by the precessional forcing (combined with eccentricity modulation) (Fig. 1e) (corr = 0.51), rather than by the 41 ka obliquity forcing (corr = -0.28). Using the time series smoothed through 100-year running mean, the composite peak of ENSO variability is  $\sim 0.40$  °C while the composite trough is  $\sim 0.30$  °C, suggesting that the fluctuation ranges roughly between +15% to -15% of its mean value. We also estimate a  $\sim 15\%$  gradual increase throughout Holocene in ORB, consistent with TRACE (see Liu et al., 2014; 10 Fig. 1d) and PMIP2/PMIP3 6 ka experiments (Masson-Delmotte et al., 2013). The in-phase relation of ENSO strength and precessional forcing is further confirmed by the power spectrum of ENSO strength (Fig.S1a, Sec 6.3) and the Hovmoller diagram (Fig. 2a, shading color). The latter shows quite uniform ENSO variation across the equatorial central-eastern Pacific, as suggested by the zonal structure of bands of strong/weak ENSO strength with 21 ka periodicity (Fig. 2a, black curve on the left), instead of 41 ka periodicity (Fig. 2a, black curve on the right). The ENSO center of action shifts between 15 the equatorial central and eastern Pacific: in TRACE there is a clear transition of Eastern Pacific ENSO to Central Pacific ENSO during Holocene (c.f. Liu et al., 2014, Extended Data Fig. 2a), in contrast, in ORB this transition on precessional time scales is not very obvious.

The annual cycle amplitude is also strongly modulated on precessional time scales (Fig. 1e), with a correlation of 0.64, while 20 having little relation with obliquity (corr=-0.13) (Erb et al., 2015). The annual cycle intensifies with increase of the precession index, consistent with TRACE and PMIP2/PMIP3 6 ka experiments (Liu et al., 2014; Fig. 1e). As shown in the time series and Hovmoller diagram, the annual cycle follows the precessional forcing in the last 300 ka (Fig. 2b) more closely than ENSO does, except for the eastern edge of the Pacific where the coastal upwelling process could be more dominant. The change in amplitude of equatorial annual cycle can be understood as the precession-dominated change in 25 annual cycle of insolation over the subtropical South Pacific. With an increased precession index (e.g., the last  $\sim 10$  ka), the annual cycle of insolation is intensified in the SH; this leads to an increased seasonal cycle of SST in the subtropical South Pacific, and eventually an increased annual cycle in the eastern equatorial Pacific (Liu et al., 2014) through the coupled air-sea processes (Liu and Xie, 1994). Specifically, we find that the precessional modulation in the subtropical South Pacific annual cycle is in phase with equatorial Pacific annual cycle (and clearly, out of phase with subtropical North Pacific annual 30 cycle) with a small lead over the entire simulation (Fig. S2).

In short, the evolutions of amplitude of ENSO and seasonal cycle both demonstrate a much closer relationship with the precessional forcing, rather than the obliquity forcing, which is consistent with Timmermann et al. (2007) in an independent model ECHO-G. Nevertheless, the in-phase relationship between them shed doubt on the previous proposed nonlinear

mechanism (frequency entrainment). In the next section, we will address this issue and develop the points on how orbital forcing induces precessional cycles of ENSO variability in ORB.

## 4 Orbital forcing mechanisms

### 4.1 Are nonlinear mechanisms working?

5 To examine the orbital forcing mechanism, we first test the nonlinear mechanism of frequency entrainment (Liu, 2002), which is found to trigger abrupt changes of ENSO variability on precessional time scales in an accelerated orbital forcing transient simulation (Timmermann et al., 2007) with similar experimental design as ORB, using an ECHO-G model. In the context of frequency entrainment, the ENSO is regarded as a nonlinear oscillatory system periodically driven by the external signal with its forcing frequency close to the intrinsic ENSO frequency (i.e. the equatorial annual cycle). When a strong  
10 annual cycle is present, nonlinear response of the ENSO oscillation tends to be dampened in energy of its intrinsic frequency, and results in a smaller amplitude. In the study of Timmermann et al. (2007), the amplitude of ENSO evolves completely out of phase (anti-phase) with that of the annual cycle on the precessional time scale (Fig.3b). This led them to hypothesize that ENSO is forced by the precessional forcing through the interaction between the seasonal cycle and ENSO via frequency entrainment. In contrast, here, the strength of ENSO evolves in phase with that of the annual cycle (Fig.1d,e;  
15 Fig.2). Therefore, the change of ENSO cannot be caused predominantly by its interaction with the seasonal cycle through frequency entrainment.

In order to compare the two model simulations more clearly, we plot the CCSM3 Nino3.4 SST in its time-evolving Morlet wavelet spectrum (Fig.3a) the same as in ECHO-G (Fig. 3b, which is the Fig. 2 of Timmermann et al., 2007). The  
20 interannual variability in both models exhibit a pronounced biennial peak rather than an observed broad 2-7 year period (e.g. Latif et al.,1998), in spite of the annual mean flux adjustment in ECHO-G (Timmermann et al., 2007) and the absence of such adjustment in CCSM3 (Deser et al., 2006; Liu et al., 2014). The different relationship between the amplitudes of ENSO and annual cycle in the two models seems to be caused more by the difference in the phase of the annual cycle than ENSO, while, indeed, the annual cycle in ECHO-G peaks around 5 ka after present, 16 ka, 40 ka, 70 ka, 90 ka, 110 ka and 130 ka  
25 BP, but the annual cycle in CCSM3 peaks about 5-10 ka later, at 0 ka, 20 ka, 40 ka, 70 ka, 97 ka, 117 ka and 140 ka BP. The annual cycle in CCSM3 is largely in phase with (slightly lags) the precessional index or SH perihelion and therefore can be understood as the equatorward propagation of subtropical South Pacific annual cycle (Liu and Xie, 1994) as discussed earlier. It is unclear to us what exactly determines the amplitude of the seasonal cycle in ECHO-G. In comparison, the amplitude of ENSO does not show a systematic difference between the two models. Indeed, many ENSO peaks occurs  
30 roughly in phase in the two models, for example, at around 0 ka, 20 ka, 40 ka, 55 ka, 75 ka, 95 ka, 115 ka and 135 ka BP. As a result, the intensity of ENSO appears in phase with the annual cycle in CCSM3, but out of phase with the annual cycle in ECHO-G. It should be pointed out that, although frequency entrainment cannot explain the ENSO response in CCSM3 due

to orbital modulation, it can explain the ENSO change in response to millennial meltwater forcing (Liu et al., 2014) or the retreat of Laurentide ice-sheet (Lu et al., 2016). In these two cases, the more abrupt external forcing eventually leads to a perturbation on the North-South asymmetry in the annual mean SST in the tropical Pacific, and in turn the amplitude of the equatorial annual cycle. The absence of such phenomenon in the orbital-only forcing CCSM3 simulation of both TRACE-  
 5 ORB (Liu et al., 2014) and ORB suggest that ENSO sensitivity of the nonlinear interaction with annual cycle is not robust on orbital time scales in this model.

Furthermore, we tested other recent hypothesized nonlinear mechanism that arises from observations of the tropical Pacific by which ENSO interacts with annual cycle and could be affected through amplitude modulation, such as the combination  
 10 mode (Stuecker et al., 2013). However, our model does not show the similar feature in EOF and spectra analysis as in Stuecker et al. (2013) (Figure not shown). We speculate the failure of the combination mode in our simulation is the biased ~biennial ENSO frequency.

#### 4.2 BJ analysis

We next examine the evolution of linear coupled ocean-atmosphere instability in the orbital forcing run. Similar to our  
 15 previous studies (Liu et al., 2014; Lu et al., 2016), we here apply the Bjerknes stability analysis (Jin et al., 2006). The Bjerknes stability (BJ) index is used to quantitatively evaluate the role of ocean-atmosphere feedbacks and damping effects. The calculation starts from the linearized SST tendency equation in the mixed layer:

$$\frac{\partial T}{\partial t} = Q - \frac{\partial(\bar{u}T)}{\partial x} - \frac{\partial(\bar{v}T)}{\partial y} - \frac{\partial(\bar{w}T)}{\partial z} - u \frac{\partial \bar{T}}{\partial x} - v \frac{\partial \bar{T}}{\partial y} - w \frac{\partial \bar{T}}{\partial z}, \quad (1)$$

where the overbar denotes the annual mean climatology, T is sea temperature anomaly, Q is the total surface heat flux and  
 20 (u, v, w) are ocean current velocity. We average eqn. (1) spatially over a rectangular box of the tropical central and eastern Pacific Ocean (5°S~5°N, 180°E~80°W) and integrate above the mixed-layer depth (~90m) following Kim and Jin (2011a,b). Denoting the averaged variables in  $\langle \rangle$ , it becomes:

$$\frac{\partial \langle T \rangle}{\partial t} = \langle Q \rangle - \left( \frac{(\bar{u}T)_{EB} - (\bar{u}T)_{WB}}{Lx} + \frac{(\bar{v}T)_{NB} - (\bar{v}T)_{SB}}{Ly} \right) - \left\langle \frac{\partial \bar{T}}{\partial x} \right\rangle \langle u \rangle - \left\langle \frac{\partial \bar{T}}{\partial z} \right\rangle \langle H(\bar{w})w \rangle + \left\langle \frac{\bar{w}}{H_1} \right\rangle \langle H(\bar{w})T_{sub} \rangle, \quad (2)$$

where

$$25 \quad H(x) = \begin{cases} 1, & x \geq 0 \\ 0, & x < 0 \end{cases},$$

is the step function. Assuming we have:

$$\frac{\partial \langle T \rangle}{\partial t} \approx R \langle T \rangle,$$

then the BJ index (R) can be derived as:

$$R = -\alpha_s - \alpha_{MA} + \mu_a \beta_u \langle -\bar{T}_x \rangle + \mu_a \beta_w \langle -\bar{T}_z \rangle + \mu_a \beta_h \langle \frac{\bar{w}}{H_1} \rangle \alpha_h, \quad (3)$$

TD    MA    ZA            EK            TH

while in eqn. (3) the coefficients can be calculated using least-square regression method (Kim and Jin, 2010 a, b; see also Liu et al., 2014 Methods for more details).

5

The BJ index represents the total feedback strength, which is a sum of five feedback terms, including two negative feedbacks, the surface heat flux feedback, or thermodynamic damping (TD), the mean advection feedback, or dynamic damping (MA), and three positive feedbacks, the zonal advection feedback (ZA), the Ekman local upwelling feedback (EK), and the thermocline feedback (TH). Each of the three dynamical positive feedbacks is the product of the background state (10  $(d_x \bar{T}, d_z \bar{T}$  and  $\bar{w})$ ), the atmospheric response sensitivity (or surface wind stress sensitivity) to SST ( $\mu_a$ ), and the oceanic response sensitivity to equatorial surface wind stress ( $\beta_u, \beta_w$  and  $\beta_h$ ), reflecting the critical role of each element in the generation of the feedback.

We made two small improvements over the method of feedback calculation of Liu et al (2014). One is the use of column (15 integrated (within top ~90m) temperature and velocity for surface layer heat budget instead of the surface layer alone. This way, the overestimation of mean advection damping (which is largest at the surface) is reduced. The other is the use of sea surface height (SSH) to estimate thermocline depth instead of heat content which was poorly estimated by column-weighted sea temperature of only three layers (surface, 56m and 149m). The positive thermocline feedback is thus more realistic. Overall, the BJ index using the new method varies roughly within the limit from -0.6 to 0 yr<sup>-1</sup>, while shifts to positive at the (20 very end of the orbital forcing simulation (Fig. 4a, purple curve). The negative BJ denotes a weakly stable ENSO mode, but we focus only on the relative change of BJ index to refer the change of ENSO growth rate in the simulation.

The robustness of the BJ index terms is tested following analysis of Graham et al. (2014). Since the BJ terms only represent the linear terms in the SST tendency equation, and exclude the nonlinear and residual terms, their contribution is calculated. (25 The correlation between evolution of mixed layer temperature tendency and the linear terms is between 0.75 and 0.85, and only increases slightly while including the nonlinear terms (e.g., Fig. S3). Thus it can be concluded that the linear mechanism dominates the growth of ENSO, while the contribution from nonlinear mechanism is negligible and the residual (including high frequency stochastic forcing) is not important. The source of error in the BJ index can also result from the use of regression coefficients in constructing the BJ feedbacks. The largest uncertainty is associated with the estimate of (30 regression coefficients of the thermocline feedback, while the Ekman feedback that is the greatest contributor to the trend of total BJ index (see the discussion below) has the least uncertainty (Fig. S4).

A comparison of the BJ index and ENSO amplitude shows that the orbital scale change in ENSO intensity can be largely explained by the BJ index, both of which vary in-phase in precessional cycles (Fig. 4a). In addition, the correlation between ENSO and BJ index is 0.40 throughout the entire simulation and is even higher (e.g. 0.46 for 250~100 ka BP) when precessional forcing is modulated by larger eccentricity. Both the ENSO variability and the BJ index show pronounced precession signals on the frequency domain (Fig. S1a and Fig. S8a, and Sec 6.3). A comparison of evolutions of BJ index in ORB and in its unaccelerated counterpart (TRACE-ORB, Liu et al., 2014) suggest that the acceleration technique could make the orbital forcing signal less robust, specifically because of delayed and dampened response below the surface ocean, thus leading to a decrease of the correlation (See more details in Sec 6.1).

To better understand the change in BJ index, the total feedback (BJ index) is decomposed into individual feedbacks in Fig. 4b. The Ekman upwelling feedback, the thermocline feedback and the zonal advection feedback all vary in phase with ENSO amplitude evolution and the BJ index, with a dominant contribution from the former two feedbacks. The heat flux damping and the mean advection damping, on the other hand, appear to be out of phase with ENSO evolution and BJ index.

The evolution of each BJ feedback is further factored as the product of the atmospheric response (to SST) sensitivity ( $\mu_a$ ), the oceanic response (to atmospheric forcing) sensitivity ( $\beta_u$ ,  $\beta_w$  and  $\beta_h$ ), and the mean state ( $d_x \bar{T}$ ,  $d_z \bar{T}$  and  $\bar{w}$ ), as shown in Fig. 5 in the left, central and right columns. Here, for convenience of comparison of the contribution of each process to the variation of the feedback evolution, the y-axis limit (on the right of each panel) is scaled with the same extent of relative change. The changes of the Ekman upwelling feedback and thermocline feedback are dominated by the atmospheric response to SST anomaly ( $\mu_a$ ), and the upwelling response and the thermocline tilt response to the surface wind anomaly ( $\beta_w$  and  $\beta_h$ ). The mean state change, especially the mean stratification  $d_z \bar{T}$ , which is found important for the change of Ekman upwelling feedback (Liu et al., 2014), only contributes modestly to the Ekman feedback term (as seen from the relatively smaller amplitude (accounts for ~10% relative change) than the parameters  $\beta_w$  and  $\mu_a$  (~20% relative change)).

The change of stratification can be seen in the composite of tropical mean climate difference between all the epochs of minimum precession index (e.g. early Holocene, weaker ENSO) and maximum precession index (e.g. present day, stronger ENSO). It suggests that the basic feature is a weaker mean stratification in most of the equatorial Pacific (Fig. S2). This can be understood as ventilation of the warmer SST signal from extratropical Southern Pacific in austral winter at perihelion (when precession index reaches a minimum) (Liu et al., 2014). Indeed, the precession signal in the evolution of the mean stratification is less pronounced in the accelerated simulation (reduced by ~30%), when comparing the amplitude of last 21 ka of red curve with grey curve (Fig. 5f). The less important role of mean stratification in Ekman pumping feedback may therefore be caused by the acceleration technique: in real time, it takes decades for the subtropical Pacific Ocean to affect the equatorial temperature through the subduction process (Huang and Liu, 1999); in the accelerated time

will be equivalent to several thousands of years (Fig. 1b), during which the extreme precessional forcing effect is likely to be smoothed out (See more details in Sec 6.1).

This change of stratification may also explain the precession induced change of thermocline response sensitivity to surface wind stress anomaly:  $\beta_h$ . In the framework of a reduced gravity model (where  $g' = g\Delta\rho/\rho$ ),  $\frac{\partial u}{\partial t} - fv = -g'\frac{\partial h}{\partial x} + \tau_x$ ,  $\frac{\partial u}{\partial t}$  can be neglected for the slow modulation on orbital time scales as in an equilibrium system, and  $fv$  is likely to be small on the equator. Thus, the dominant balance leads to  $\frac{\partial h}{\partial x} = \tau_x/g'$ . A decrease of the reduced gravity  $g'$  corresponds to a weaker stratification, and can lead to a larger tilt response  $\frac{\partial h}{\partial x}$  forced by the same  $\tau_x$ , implying a larger  $\beta_h$ .

To this point, however, the linkages between the precessional forcing and the response sensitivity  $\mu_a$  and  $\beta_w$  remain not very clear.  $\beta_w$  is complex because the upwelling response is affected by stratification, and Ekman upwelling processes in a stratified fluid is difficult to represent in simple dynamic balances. For  $\mu_a$ , more clues in surface climate sensitivity are needed to answer why 21 ka signal is more obvious than 41 ka signal, as obliquity intuitively controls the annual mean SST in the tropics thus the wind response to SST anomaly (Roberts, 2007).

### 4.3 Stochastic forcing mechanisms

It has been suggested that ENSO can be generated or its intensity significantly changed by the stochastic climate forcing (e.g. Thompson and Battisti, 2001a,b). The stochastic high-frequency variability, such as the Madden-Julian Oscillations (MJO) and westerly wind bursts (WWBs) in the equatorial western Pacific (e.g. Kapur et al., 2011), or midlatitude atmospheric variability such as the North Pacific Oscillation over the North Pacific (Vimont et al., 2001; 2003), can trigger or enhance an ENSO activity. In particular, Chiang et al. (2009) argued that a reduction of stochastic forcing from the extratropics leads to the reduction of ENSO during the mid-Holocene in their idealized sensitivity experiments, which is driven only by insolation changes outside the deep tropical Pacific. Although it is estimated from the heat budget equation that the residual terms (including the high-frequency stochastic forcing) only have a secondary compared with the BJ feedback terms (Sec 4.2), below we try to quantify how the noise is modulated by the orbital forcing and its connection to ENSO strength.

The daily variance of stochastic forcing (mechanical forcing) is derived from the monthly output of surface zonal wind speed  $\bar{u}$  and squared zonal wind speed  $\overline{u^2}$  (using 500 hPa meridional wind exhibits a similar result, Figure not shown). The monthly mean of  $u$  daily variance is calculated as:  $\sum_{n=1}^N u_n^2/N = \overline{u^2} - \bar{u}^2$ , while  $\overline{u^2} = \sum_{n=1}^N (\bar{u} + u_n)^2/N$ , and  $\bar{u} = \sum_{n=1}^N (\bar{u} + u_n)/N$  ( $\sum_{n=1}^N u_n = 0$ ), where  $N$  is the number of days in one month and  $u_n$  is the daily anomaly to monthly mean of zonal wind speed. To show its trend which represents the processes like MJO or WWBs activities, we calculate its

spatial average over the tropical western Pacific (TWP, depicted in Fig. S3). Our results suggest that the variance of stochastic forcing on daily time scales, in particular during the ENSO growth season of boreal spring and summer (the largest ENSO variability by season is still in winter, Figure not shown), follows closely the precessional cycles (corr=0.91, Fig. 6a, green solid line) and the evolution of ENSO variability. However, in contrast, the trend of stochastic forcing variance averaged for the rest of the months seems to be out of phase with the precessional forcing (Fig. 6a, green dashed line). It is unclear if that contradiction (see also Chiang et al., 2009) is related to modern day ‘mid-winter suppression’ phenomenon (Nakamura 1992; Nakamura et al., 2002).

The stochastic forcings on ENSO generated over North Pacific (e.g., mid-latitude storm track, or NPO variability during boreal winter) can be very different from MJO or WWBs in the TWP. Interestingly, the trend of the daily variance of stochastic forcing averaged over the North Pacific storm track region (NP, depicted in Fig. S3) turns out to be similar to that of the TWP (corr=0.61, Fig. 6b, also note the similar ‘mid-winter suppression’ contradiction that correlation is decreased in winter), making the point that the stochastic forcing could contribute to the ENSO evolution from either source. In this case, their consistent slow modulations to orbital forcing simply imply both are responding to the orbital forcing in the same way, therefore we don’t know, from this analysis, which is the driving stochastic forcing on ENSO evolution.

One important mechanism that allows the extratropical atmospheric variability to influence ENSO is the Pacific Meridional Mode (PMM). The PMM, independent of ENSO, represents the North Pacific atmospheric variations that communicates to the tropical Pacific (Vimont et al., 2001) and may trigger ENSO events in the present day observation (Chang et al., 2007). In the case of paleo ENSO, the PMM has also been suggested to contribute to the weakened ENSO during the mid-Holocene, with the PMM variance reduced by ~40% from the present day, in qualitative agreement with ENSO activity reduction (Chiang et al., 2009). We have examined the PMM and the related NPO following Chiang et al (2009). Although there are significant changes of both PMM and NPO at precessional time scales, their phase does not seem to be aligned with the ENSO intensity very well (Figure not shown). Therefore, in our model, the role of extratropical stochastic variability on ENSO is not very clear. Further analysis including model simulation with higher spatial (capable of resolving processes like MJO) and temporal (daily or hourly) resolution, as well as better physically reproduced ‘pathways’ or ‘teleconnections’ that communicate the remote forcing of stochastic noise is called for to fully address this issues and to confirm our hypothesis, in addition to improve our understanding on stochastic noise in response to precessional forcing.

## 5 GHGs and ice-sheet forcing mechanisms

We now further study the response of ENSO to the slowly varying GHGs forcing and ice-sheet forcing in the last 300 ka. It has been noted that in TRACE experiments of the last 21,000 years an increase of deglacial atmospheric GHGs concentration tends to weaken ENSO. Nevertheless, on glacial-interglacial timescale, the variation of GHGs level is

5 accompanied by a large change in glaciation, with a retreating glacial ice sheets corresponding to high GHGs period (Fig. 7b,c). Furthermore, sensitivity experiments show that the lowering of continental ice sheet can impact the tropical coupled ocean-atmosphere system significantly (e.g., Russell et al. 2014; Lee et al. 2014), leading to an intensified ENSO (Liu et al., 2014; Lu et al., 2016). As such, the effect of changing GHGs and ice-sheet may compensate each other during deglacial evolution, at least in CCSM3 (Liu et al., 2014).

Here, two sensitivity experiments are performed by adding on top of the orbital forcing the equivalent CO<sub>2</sub> forcing (ORB+GHG), and furthermore the continental ice sheet (ORB+GHG+ICE). The prescribed forcing and boundary conditions for ORB+GHG and ORB+GHG+ICE are shown in Fig. 7(a-c). During the past 300 ka, the GHGs level (Fig. 7b) and global ice-sheet volume (Fig. 7c) are both dominated by three quasi-100 ka cycles (Petit et al., 1999), but largely in the opposite phase with a higher GHGs accompanied by a reduced ice sheet. In addition, each cycle is characterized by a ‘sawtooth’ shape evolution, with, for example, a slowly decreasing trend followed by a rapid recovering turn towards its maximum level for GHGs.

15 ENSO strength and annual cycle amplitude of ORB, ORB+GHG and ORB+GHG+ICE are shown in Fig. 7d and e, respectively. First of all, the most striking feature is that the modulation of ENSO in ORB+GHG and ORB+GHG+ICE (Fig. 7d) is modulated predominantly by the precessional forcing (Fig. 7a) (tested by power spectrum, Fig. S1b,c), although the mean climate evolves in the 100 ka glacial cycles. This precession modulation of ENSO variance resembles closely to that in ORB (Fig. 7d), even when GHGs and ice-sheet forcings are included, and is consistent with the previous study in TRACE (Liu et al., 2014). Second, a further examination shows some modest responses of ENSO to GHGs and ice sheets. Starting from 300 ka BP onward to ~250 ka BP, as GHGs decreases (from 250 to 200 ppm, Fig. 7b), ENSO amplitude in ORB+GHG (from 0.3 to 0.45, Fig. 7d, red) is enhanced relative to that in ORB (from 0.3 to 0.35, Fig. 7d, black), and then stays strong throughout. When the accompanied expansion of ice sheet ( $2 \times 10^6 \text{ km}^3$ ) is further imposed (Fig. 7c), however, the amplitude of ENSO (in ORB+GHG+ICE, Fig. 7d, blue) is reduced from that in ORB+GHG back to a level comparable with that in ORB, both to 0.35. This sign of change in ENSO variance is consistent with a compensation between GHGs and ice sheet during the last deglaciation (Liu et al., 2014). In particular, the three simulations tend to be closer at the full interglacial (marked by three grey vertical bars in Fig. 7 and Fig. 8, and the last is the pre-industrial epoch), when the GHGs level and ice-sheet conditions are roughly the same as during the pre-industrial.

30 The effect of GHGs and ice sheet forcing on ENSO can be seen more clearly in the difference of the amplitudes of ENSO and annual cycle between ORB+GHG and ORB (Fig. 8a, red curve), and between ORB+GHG+ICE and ORB+GHG (Fig. 8b, red curve), respectively. The results are also qualitatively consistent with the analysis in TRACE (Liu et al., 2014). The modulation of ENSO tends to be out of phase with the annual cycle (Fig. 8, red vs. blue), the GHGs concentration and ice-sheet volume (Fig. 8, red vs. grey). The GHGs change, predominantly in the 100 ka cycles, leads to an in-phase change of

the annual cycle amplitude and an out-of-phase change of the ENSO amplitude, and it can be interpreted as follows. The increased GHGs concentration leads to an asymmetric annual mean warming (a stronger warming north of the equator) in the tropical Pacific (Figure not shown), which enhances the equatorial asymmetry and in turn the annual cycle (Timmermann et al., 2004). The enhanced annual cycle then weakens ENSO through frequency entrainment (Liu, 2002). The ice sheet change, also predominant in the 100-kyr cycle, forces an in-phase change of annual cycle intensity and an out-of-phase change of ENSO intensity. The larger continental ice sheet corresponds to a stronger annual cycle and weaker ENSO, which can be explained as follows. A smaller extent of NH ice-sheet leads to northward displacement of NH jet stream, increased sea ice coverage over the North Atlantic and North Pacific, and a resultant cooling over the equatorial northeast Pacific (Lu et al., 2016), and in turn a weaker annual cycle. The weaker annual cycle then intensifies ENSO through the nonlinear frequency entrainment (Liu, 2002).

To further examine the mechanisms of GHGs and ice-sheet forcing on ENSO variability change, we calculate the trend of ENSO linear growth rate (BJ index, Fig. S4) for ORB+GHG and ORB+GHG+ICE (the same as for ORB, Sec 4.2). The correlation of BJ index and ENSO variability as well as the coherence of BJ index and external forcing (Fig. S5) is analysed to understand their relationship with respect to the time space and frequency domain, respectively. We first show that the correlation between ENSO variability and its corresponding BJ (Fig. S4) is 0.40, 0.50, 0.31 (0.43, 0.52, 0.33 for 250-100 ka BP) for ORB, ORB+GHG and ORB+GHG+ICE, respectively. Physically, the aforementioned nonlinear mechanisms of GHGs and ice-sheet forcing are expected to decorrelate the linear correlation. For instance, the nonlinear terms in the SST tendency equation can have a larger contribution, so the linear terms that the BJ index represents will have a poorer correlation with the ENSO anomaly. That is exactly the case for the ice-sheet forcing (Fig. S4b,c, from 0.50 to 0.31 after including ice-sheet forcing). In addition, within the frequency domain the BJ trend in ORB+GHG+ICE exhibits only one coherence peak at ~21 ka (Fig. S5c) induced by the precessional forcing (as in Fig. S5a), leaving little signal at ~100 ka period which is the within the dominant frequency domain of GHGs and ice-sheet forcing. However, the mechanism of ORB+GHG seems to be more complex, as suggested by the increase of correlation when including GHGs forcing (Fig. S4a,b, from 0.40 to 0.50). The statistical test determines two coherence peaks in BJ index in ORB+GHG, one at ~21 ka for orbital precessional forcing and the other at ~100 ka for GHGs forcing, but only the former exceeds a statistically significant threshold (Fig. S5b). We speculate that a more diffusive equatorial thermocline is forced by the CO<sub>2</sub> warming at the sea surface (Meehl et al., 2006), and that process leads to a less stratified upper ocean therefore weakening the Ekman upwelling feedback and thermocline feedback (just opposite to the discussion in Sec 4.2) associated with the ENSO linear growth rate. In short, in CCSM3, the GHGs and ice-sheet forcing on ENSO amplitude has a compensation; the increased GHGs concentration leads to weakened ENSO and the retreat of ice-sheets leads to intensified ENSO. The results qualitatively show the dominant forcing mechanism on ENSO variability for both GHGs and ice-sheet are the nonlinear frequency entrainment.

## 6 Discussion

### 6.1 Acceleration effect and model performance

The effect of the accelerated boundary conditions (orbital parameters) on the climate evolution here is estimated first using a one-dimensional diffusive ocean model (Timm and Timmermann, 2007). The simple diffusive process shows how the temperature profile responds to a surface forcing:

$$\frac{\partial T(z)}{\partial t} = -\frac{\partial}{\partial z} \left( \kappa(z) \frac{\partial T(z)}{\partial z} \right) + F(z=0, t).$$

For simplicity, the turbulent background diffusion for the global ocean is prescribed as  $\kappa = 6.2 \times 10^{-5} \text{m}^2 \text{s}^{-1}$ . The periodic forcing  $F$  is prescribed at ocean surface as  $F(z=0, t) = A \sin(\omega t)$ . The propagation of the forcing is shown in Fig. S9 for 100-fold acceleration  $\omega_{100} = 2\pi/210 \text{ yr}^{-1}$ , 10-fold acceleration  $\omega_{10} = 2\pi/2100 \text{ yr}^{-1}$  and non-acceleration  $\omega_1 = 2\pi/21000 \text{ yr}^{-1}$ . The results for the three scenarios of forcing frequencies depict the in-phase temperature anomalies at the surface on a common time axis (stretched by a factor of 100 and 10 for (a) and (b)). The acceleration leads to dampened and delayed response in the deep ocean. The phase lag grows with depth, by 10-fold acceleration is about 600 accelerated years at 200m depth, while by 100-fold acceleration is about 2000 accelerated years (2 ka). It is obvious the increased factor of acceleration could weaken the surface anomalies that propagate through deep ocean, thus twisting the phase relationship between the deep ocean and the surface forcing.

Furthermore, we make a direct comparison between the last 210-year of the 3000-year accelerated (ORB, representing the last 300 ka) with the 21000-year unaccelerated (TRACE-ORB, last 21 ka, Liu et al., 2014) orbital single-forcing simulation. We will focus on the orbital time scale temporal characteristics of the climate mean state and variability. The relative change of decadal mean SST over the eastern equatorial Pacific (EEP) of ORB is almost identical with that of TRACE-ORB (Fig. 1c, grey vs. red), with no phase difference and an amplitude of  $0.4^\circ\text{C}$ , which is dominated by the signals from the change in the obliquity (Fig. 1b). Likewise, the N-S SST gradient in the EEP (Fig. 1e, grey vs. red) and annual cycle amplitude (Fig. 1g, grey vs. red) in the two simulation suggest no much difference in amplitude (both are  $0.25^\circ\text{C}$  or  $0.3^\circ\text{C}$ , respectively) or phase. It can be concluded that the tropical climate and surface ocean can be immediately influenced by surface flux anomalies and reach quasi-equilibrium under accelerated forcing (Timm and Timmermann, 2007; Timmermann et al., 2007). However, similar to results in the simple diffusive model, the intermediate/deep sea temperatures in CCSM3 are biased by the acceleration technique because of their slow response time. Fig. 1d (grey vs. red) depicts the evolution of subsurface temperature in the EEP in the two simulations, and their systematic differences are noticeable. The unaccelerated simulation shows larger forced precessional signals (an amplitude of  $0.4^\circ\text{C}$  vs.  $0.2^\circ\text{C}$ ) and leads in phase by  $\sim\pi/4$  (or 5 ka, larger than that in the simple diffusive process). The longer adjustment time of subsurface ocean than surface ocean induces the delayed response (Timm and Timmermann, 2007) which tend to cancel out the opposite effect below surface water between two successive extreme precessional forcing cases. The simulated ENSO evolution in the accelerated and unaccelerated simulations both depict considerable intrinsic variability (Fig. 1f, see also Sec 6.3), but they are fairly consistent in their

phase (both in phase with precession index) and amplitude ( $0.1^{\circ}\text{C}$ ). The orbital time scale change of ENSO variability is dominated by the  $\sim 21$  ka precessional forcing, as confirmed by its power spectrum.

In addition to the consistent amplitude of EEP annual cycle in ORB and TRACE-ORB, the simulated phase of EEP annual cycle is in agreement with other simulations, which further suggest the quasi-equilibrium of surface climate in the accelerated simulation. For example, some snapshots simulations (all reach equilibrium) in GFDL-CM2 model (Erb et al., 2015) show that the phase of SST annual cycle under Autumnal Equinox, Winter Solstice, Vernal Equinox and Summer Solstice extreme precessional forcing is shifted, and the phenomenon also occurs in ORB (Figure not shown). For simulated ENSO in CCSM3, its biennial frequency bias is not affected by the acceleration (Sec 4.1). But it is interesting that the seasonal phase locking of ENSO variance is also shifted by precession modulation in ORB, which is qualitatively consistent with another CCSM4 snapshot simulation (Karamperidou et al., 2015). Overall, these evidences suggest the accelerated simulation has a reasonable performance for the tropical Pacific, at least for the surface mean climate. More detailed analysis on precession modulated phase shift is beyond the scope of this study, and will be presented in a separate paper (Lu and Liu, 2017).

We have argued that orbital forced signal in the coupled ocean-atmosphere instability is the main driver of the evolution of ENSO intensity (see Sec 4.2). The effect of acceleration technique is thus examined with respect to BJ index. Each term of BJ index (Fig. 4b, short 21 ka curves for TRACE-ORB, longer curves for ORB) and their components (Fig. 5, grey curves for TRACE-ORB, curves with other colors for ORB) are compared for the two simulations, and they are qualitatively comparable. The major offset in the BJ index (Fig. 4b, purple) that the acceleration induces is the weakened precessional scale signal characterized by smaller amplitude and incomplete cycles, for example, the amplitude of BJ index is reduced by  $\sim 50\%$  in the accelerated simulation. The difference in BJ index associated with acceleration is mainly introduced by change (weakened precessional signal) in Ekman upwelling feedback (Fig. 4b, red) and thermocline feedback (Fig. 4b, brown), both reduced by  $\sim 50\%$ , due to similar feature of upper ocean stratification (weakened precessional signal and less stratified) (Fig. 5f), and the resultant oceanic response  $a_h$  (weakened response of entrainment temperature to anomalous thermocline depth) (Fig. 5d, grey curves).

In brief, the acceleration technique shows difficulties mainly due to the damped and delayed response to boundary conditions (orbital parameters) below surface ocean, otherwise the simulation results are in good agreement with the unaccelerated counterpart. The tropical Pacific mean climate at the ocean surface is not affected by the acceleration. For change in ENSO variability that could be partly influenced from weakened precessional signal in the subsurface ocean, the acceleration is expected to lower the robustness of our proposed mechanism.

At last, we acknowledge the potential setbacks that the acceleration technique could bring about, and the diminishing applicability of a relatively problematic accelerated model to the real world. Still, our results provide an example to study ENSO sensitivity under extreme orbital forcing on centennial time scales in the transient climate evolution, which was rarely studied in previous researches. It is obvious that even the 100-fold accelerated orbital time scales, say, ~210-year for precession and ~410-year for obliquity are far longer than that of typical tropical surface climate processes, e.g., the annual cycle and ENSO.

## 6.2 Different initializations and forcing combination

In addition to the acceleration, when comparing TRACE simulations with the three accelerated 300 ka simulations, one should notice that the two sets of experiments uses different initialization methods. TRACE simulations (including TRACE and four single sensitivity runs) was initialized from a LGM equilibrium state (Liu et al., 2014, Method), while the three accelerated runs were all spun up from a Pre-industrial state. An obvious difference PI and LGM initializations introduces is that the temperatures in 300 ka ORB simulation are systematically higher than TRACE-ORB simulation. For example, the EEP SST and subsurface sea temperature are higher in ORB by 1°C and 1.5°C (Fig. 1c) and the vertical temperature gradient in the upper ocean smaller (0.5°C in 50m, or 0.01°C/m, Fig. 1c,d; Fig. 5f). Despite changes in the mean state, the tropical annual cycle amplitude is largely not affected (Fig. 1g). While ENSO intra-model variability is almost unchanged, its overall variability is slightly increased by 0.05°C in a warmer state (Fig. 1f).

A higher global temperature, however, may help to explain some ENSO behaviors that appears in TRACE while missing in 300 ka simulations. For instance, in TRACE-ICE single forcing simulation, an abrupt intensification of ENSO variability is observed around 14 ka BP when the thickness of Laurentide ice sheet reduced a large amount to its intermediate height (Lu et al., 2016). However, the feature is not obvious in ENSO in ORB+GHG+ICE or in ENSO offset of ORB+GHG+ICE from ORB+GHG during the prescribed deglaciation. One possibility is the cooler mean state in TRACE-ICE than in ORB+GHG+ICE induced by two different initializations and different GHG levels (fixed at LGM level in TRACE-ICE, transient in ORB+GHG+ICE). Cooler temperature favors the formation of sea-ice at Northern Hemisphere high latitude, for example, there is substantial cooling in the North Pacific and North Atlantic during the interglacial (0 ka BP in TRACE-ICE), which is absent in ORB+GHG+ICE. The expansion of sea ice is found to be an important contributor to the interhemispheric asymmetry that compensates the loss of continental ice sheets (mainly in the NH) in terms of surface heat budget, and helps to weaken the annual cycle thus intensifying ENSO (Lu et al., 2016). From a pre-industrial initialization and at a relatively high GHG level, it would be difficult for sea-ice expansion of such an extent and abruptness (Figure not shown).

The PI initialization in 300 ka simulations may also lead to climate drift during the initial period, which makes interpretation of long term climate change of our transient simulations difficult. For example, at the beginning of the simulation the EEP

SST is  $\sim 24.7^{\circ}\text{C}$ , and for the first 700 model years there appears to be a decreasing trend, towards  $\sim 24.5^{\circ}\text{C}$  at the end of the simulation (Fig. 1c). A slightly decreasing trend is also seen in the EEP subsurface temperature (Fig. 1d). However, the bias should not affect our analysis on the climate change on orbital time scale, as both the obliquity scale EEP SST signal and precessional scale EEP subsurface temperature, ENSO and annual cycle are quite robust. At least for the later period of the simulation our model clearly reaches an equilibrium state (e.g. last 2000 model years), and such drifts have become acceptably slow because climatic metrics such as ENSO and annual cycle in accelerated ORB are quantitatively comparable with TRACE-ORB.

It should also be pointed out that the difference between the set of TRACE experiments and the set of 300-kyr experiments here can be caused not only by the acceleration, but also by the different forcing combination. In TRACE, each single forcing is imposed individually, with all the other conditions held at 19ka BP. Here, the GHGs and ice sheet forcing are added on to the orbital forcing one by one, with other conditions held constant at pre-industrial. Therefore, the isolation of forcing of GHGs and ice sheet, such as the discussion on Fig. 8 by subtraction of physical derivations of two simulations, works only if the process is linear, which is unlikely to be true. In spite of the differences, however, it seems that the major conclusions here are consistent with TRACE, suggesting the proposed mechanism of GHGs and ice sheet forcing on ENSO in CCSM3 is somewhat robust.

### 6.3 Intra-model ENSO variability

It has been widely observed, with modest or without change in external forcings, that multidecadal fluctuations in simulated ENSO behavior can still occur in CCSM3 (Liu et al., 2014) or other CGCMs (reviewed by Wittenberg, 2015). In our 300 ka simulations, modeled ENSO variability indeed undergoes fluctuations from decadal to multidecadal (model-year) time scale (Fig. S6b, grey line). However, by smoothing out the modeled intrinsic ENSO variability, we demonstrate that the evolution of orbital time scale ENSO variability is evidently associated with the change in the precessional parameter (Fig. S6a), with the former either represented by ENSO in 10-year windows smoothed over 100 years (Fig. S6b, black line), or ENSO in 100-year windows (Fig. S6b, red line). The correlation between the precessional forcing and ENSO variability is 0.49 and 0.47 for the two methods, respectively, although it can be implied that the correlation has already been reduced by the acceleration technique that dampens the precessional signal below the ocean surface (Sec 6.1) or the climate drift during the initial period (Sec 6.2).

Furthermore, the power spectrum for the time series of ENSO amplitude is calculated (Fig. S1a), and its  $\sim 21$  ka frequency peaks pass 95% significance level. It confirms that the primary change in ENSO amplitude is following the precessional forcing. In addition, as we argued in the manuscript, the relative change of ENSO amplitude in Mid-Holocene ( $\sim 6$ ka) to pre-

industrial is in the within the range of PMIP snapshots as that of TRACE experiment. These evidences are enough to support our argument against the no forcing null hypothesis.

5 Finally, it should be pointed out that the biased ENSO frequency (i.e. the quasi-biennial ENSO in CCSM3) in our model actually strengthen the robustness of our result because more ENSO events could occur between the two extreme precessional phases. For instance, each  $\sim 21$  ka (equals  $\sim 210$  model years) precessional cycle could have around 100  $\sim 2$ -year ENSO cycles, which increases the sample size compared to around 50  $\sim 4$ -year ENSO.

## 7 Summary and implications

10 This paper mainly aims to investigate the forcing mechanism for the slow (about orbital time scale) evolution of ENSO and to determine the constraints on the climate sensitivity during late-Pleistocene. The deep-time (300 ka BP to PD) that the simulations in our study represent (although the acceleration technique is applied) gives us more confidence in understanding paleo ENSO forcing mechanisms, especially when our previous unaccelerated (21 ka BP to PD) full and single-forcing simulations (TRACE) are also taken into account. The sensitivity of ENSO to orbital forcing variations is found to dominate the overall ENSO evolution during the last 300,000 years with a sole significant frequency peak, while the offset induced by 15 GHGs forcing and ice-sheet forcing leaves a much smaller signal.

The orbital modulation of ENSO characteristics, as revealed in ORB simulation, is consistent with TRACE-ORB and PMIP snapshots. The ENSO variability shows pronounced  $\sim 21$  ka precessional cycles, with the amplitude of equatorial annual cycle varying coherently, while the influence of obliquity is not evident. The orbital forcing influences ENSO amplitude 20 through changes in the positive ocean-atmosphere feedbacks, among which Ekman upwelling feedback and thermocline feedback contribute the most (but the latter has a much larger uncertainty). Similar to TRACE, the precessional forcing on the subtropical South Pacific causes changes in the tropical Pacific stratification. While stratification is an important component in determining the strength of Ekman upwelling feedback, it further alters the responses of ocean upwelling and thermocline tilt to the wind anomaly, modifying Ekman upwelling feedback and thermocline feedback, respectively. The 25 100-fold acceleration is found to dampen and delay the precession signal below the surface ocean, by about half of the amplitude and at least  $\pi/10$  in phase at  $\sim 100$ m depth.

We have also demonstrated that there could be precession-induced variation of stochastic forcing outside the EEP that influences ENSO variability through remote mechanisms, but only with a modest contribution (less than 40%). ENSO can be 30 driven by the external driver of weather noise either from the TWP by exciting oceanic Kelvin waves or from the North Pacific via the PMM activity. At present, it is difficult to identify which process plays a quantitatively more important role.

Despite their substantial changes, the GHGs and ice-sheet forcing are found to impose a relatively slighter influence (not significant on the power spectrum) on the prominent orbital-induced slow evolution of ENSO variation, which can be attributed to their compensation effect. The nonlinear frequency entrainment mechanism whereby a stronger annual cycle suppresses ENSO variability applies commonly in ORB+GHG and ORB+GHG+ICE. Towards the full interglacial such as pre-industrial, equatorial annual cycle can either be amplified or weakened by a more asymmetric warming around the equator due to increased GHGs concentration or a cooling north of the equator (thus more symmetric) due to the decay of ice sheets, respectively. The GHGs-induced surface warming probably also leads to a less stratified upper ocean thus weaker Ekman upwelling and thermocline feedbacks.

The results have implications to our understanding of ENSO in the past, and the simplest case could be ENSO during mid-Holocene (~6 ka BP) when there were only pronounced changes in the insolation but comparative GHGs level and ice-sheet volume compared to pre-industrial era. Neither observational records (Moy et al., 2002; Riedinger et al, 2002; Conroy et al, 2008; Cobb et al., 2013; Carre et al., 2014) nor climate modeling studies (see Roberts et al., 2014 for a summary; An and Choi, 2014) are sufficient enough, till this day, to fully address this issue, and how ENSO responds to the variations of external forcings remains debatable. We provide a perception, self-consistent within at least one complex climate model that the ENSO variability could increase gradually from the mid-Holocene to pre-industrial time due to precessional forcing. The ENSO center of action could also shift between EP and CP (Karamperidou et al., 2015). The paleoclimate community working on ENSO proxy records may need to pay attention to expanded locations from the equatorial Pacific, particularly during the Holocene. At last, our results offer a modeling constraint on ENSO evolution during the past 300,000 years.

20

Nevertheless, our results are based on a single climate model and the results should be treated with caution because of model dependence of ENSO (Masson-Delmotte et al., 2013). It is ideal that orbital/GHG/ice-sheet forcing transient experiments are reproduced using other climate models. Achieving this long term goal will provide a valuable analysis to evaluate sensitivity of climate system models to external forcing and improve our understanding of past and future climate.

## 25 **Acknowledgements**

This work is supported by Chinese NSFC41130105 and MOST2012CB955200. The authors thank two anonymous reviewers for their thoughtful comments and criticism that have helped us to improve this manuscript.

## References

- An, S. I. and Choi, J.: Mid-Holocene tropical Pacific climate state, annual cycle, and ENSO in PMIP2 and PMIP3, *Clim. Dyn.*, 43(3-4), 957-970, 2014.
- An, S. I., A. Timmermann, L. Bejarano, F. F. Jin, F. Justino, Z. Liu and A. Tudhope: Modeling evidence for enhanced El Niño–Southern Oscillation amplitude during the Last Glacial Maximum, *Paleoceanography*, 19, PA4009, 2004.
- Augustin, L., Barbante, C., Barnes, P. R., Barnola, J. M., Bigler, M., Castellano, E. and Dreyfus, G., 2004: Eight glacial cycles from an Antarctic ice core, *Nature*, 429(6992), 623-628, 2004.
- Battisti, D. S. and Hirst, A. C.: Interannual variability in the tropical atmosphere-ocean model: influence of the basic state, ocean geometry and nonlinearity, *J. Atmos. Sci.*, 45, 1687- 1712, 1989.
- 10 Berger, A. and M.-F. Loutre: Insolation values for the climate of the last 10 million years, *Quat. Sci. Rev.*, 10, 297-317, 1991.
- Bjerknes, J.: Atmospheric teleconnections from the equatorial Pacific, *Mon. Weather Rev.*, 97, 163-172, 1969.
- Carré, M. and Coauthors: Holocene history of ENSO variance and asymmetry in the eastern tropical Pacific, *Science*, 345, 1045-1048, 2014.
- 15 Chang, P. and Coauthors: Pacific meridional mode and El Niño—Southern oscillation, *Geophys. Res. Lett.*, 34, 2007.
- Chen, G. S., Kutzbach, J. E., Gallimore, R. and Liu, Z.: Calendar effect on phase study in paleoclimate transient simulation with orbital forcing, *Clim. Dyn.*, 37(9-10), 1949-1960, 2011.
- Chiang, J., Y. Fang and P. Chang: Pacific climate change and ENSO activity in the mid-Holocene, *J. Clim.*, 22, 923-939, 2009.
- 20 Christensen, J.H., K. Krishna Kumar, E. Aldrian, S.-I. An, I.F.A. Cavalcanti, M. de Castro, W. Dong, P. Goswami, A. Hall, J.K. Kanyanga, A. Kitoh, J. Kossin, N.-C. Lau, J. Renwick, D.B. Stephenson, S.-P. Xie and T. Zhou, *Climate Phenomena and their Relevance for Future Regional Climate Change*. In: *Climate Change 2013: The Physical Science Basis. Contribution of Working Group I to the Fifth Assessment Report of the Intergovernmental Panel on Climate Change* [Stocker, T.F., D. Qin, G.-K. Plattner, M. Tignor, S.K. Allen, J. Boschung, A. Nauels, Y. Xia, V. Bex and P.M. Midgley (eds.)]. Cambridge University Press, Cambridge, United Kingdom and New York, NY, USA, 2013.
- 25 Clement, A. C., Seager, R. and Cane, M. A.: Orbital controls on the El Niño/Southern Oscillation and the tropical climate, *Paleoceanography*, 14(4), 441-456. 1999.
- Cobb, K. M. and Coauthors: Highly variable El Niño–Southern Oscillation throughout the Holocene, *Science*, 339, 67-70, 2013.
- 30 Conroy, J. L., J. T. Overpeck, J. E. Cole, T. M. Shanahan and M. Steinitz-Kannan: Holocene changes in eastern tropical Pacific climate inferred from a Galápagos lake sediment record, *Quat. Sci. Rev.*, 27, 1166-1180, 2008.
- Deser, C., A. Capotondi, R. Saravanan and A. S. Phillips: Tropical Pacific and Atlantic climate variability in CCSM3, *J. Climate*, 19, 2451-2481, 2006.
- Erb, M. P., A. J. Broccoli, N. T. Graham, A. C. Clement, A. T. Wittenberg, and G. A. Vecchi: Response of the Equatorial Pacific Seasonal Cycle to Orbital Forcing. *Journal of Climate*, 28, 9258-9276, 2015.
- 35 Ford, H. L., Ravelo, A. C. and Polissar, P. J.: Reduced El Niño–Southern Oscillation during the Last Glacial Maximum, *Science*, 347(6219), 255-258, 2015.
- Emile-Geay, J., Cobb, K. M., Carré, M., Braconnot, P., Leloup, J., Zhou, Y. and Driscoll, R.: Links between tropical Pacific seasonal, interannual and orbital variability during the Holocene, *Nature Geoscience*, 2015.

- Erb, M. P., Broccoli, A. J., Graham, N. T., Clement, A. C., Wittenberg, A. T. and Vecchi, G. A.: Response of the equatorial Pacific seasonal cycle to orbital forcing, *J. Clim.*, 28(23), 9258-9276, 2015.
- Graham, F. S., Brown, J. N., Langlais, C., Marsland, S. J., Wittenberg, A. T. and Holbrook, N. J.: Effectiveness of the Bjerknes stability index in representing ocean dynamics. *Climate dynamics*, 43(9-10), 2399-2414, 2014.
- 5 Huang, B. and Z. Liu: Pacific subtropical-tropical thermocline water exchange in the National Centers for Environmental Prediction ocean model, *J. Geophys. Res.*, 104, 11,065-11,076, 1999.
- Jin, F. F.: An equatorial ocean recharge paradigm for ENSO. Part I: Conceptual model, *J. Atmos. Sci.*, 54, 811-829, 1997a.
- Jin, F. F.: An equatorial ocean recharge paradigm for ENSO. Part II: A stripped-down coupled model, *J. Atmos. Sci.*, 54, 830-847, 1997b.
- 10 Jin, F. F., S. T. Kim and L. Bejarano: A coupled-stability index for ENSO, *Geophys. Res. Lett.*, 33, L23708, 2006.
- Kao, H. Y. and Yu, J. Y.: Contrasting Eastern-Pacific and Central-Pacific Types of ENSO, *J. Clim.*, 22, 615-632, 2009.
- Kapur, A., Zhang, C., Zavala-Garay, J. and Hendon, H. H.: Role of stochastic forcing in ENSO in observations and a coupled GCM, *Clim. Dyn.*, 38(1-2), 87-107, 2012.
- Karamperidou, C., P. N. Di Nezio, A. Timmermann, F.-F. Jin, and K. M. Cobb.: The response of ENSO flavors to mid-Holocene climate: Implications for proxy interpretation, *Paleoceanography*, 30, 527-547, 2015.
- 15 Kim, S. T. and F.-F. Jin: An ENSO stability analysis. Part I: results from a hybrid coupled model, *Clim. Dyn.*, 36, 1593-1607, 2011a.
- Kim, S. T. and F.-F. Jin: An ENSO stability analysis. Part II: results from the twentieth and twenty-first century simulations of the CMIP3 models, *Clim. Dyn.*, 36, 1609-1627, 2011b.
- 20 Koutavas, A. and S. Joanides: El Niño–Southern Oscillation extrema in the Holocene and Last Glacial Maximum, *Paleoceanography*, 27, 2012.
- Latif, M., Anderson, D., Barnett, T., Cane, M., Kleeman, R., Leetmaa, A. and Schneider, E.: A review of the predictability and prediction of ENSO, *Journal of Geophysical Research*, 103(C7), 14375-14393, 1998.
- Lee S.Y., Chiang J.C. and Chang P.: Tropical Pacific response to continental ice sheet topography, *Clim. Dyn.* 44:2429–2446, 2014.
- 25 Liu, Z. and S. Xie: Equatorward propagation of coupled air-sea disturbances with application to the annual cycle of the eastern tropical Pacific, *J. Atmos. Sci.*, 51, 3807-3822, 1994.
- Liu, Z., Kutzbach, J. and Wu, L.: Modeling climate shift of El Niño variability in the Holocene, *Geophys. Res. Lett.*, 27(15), 2265-2268, 2000.
- 30 Liu, Z.: A Simple Model Study of ENSO Suppression by External Periodic Forcing, *J. Clim.*, 15, 1088-1098, 2002.
- Liu, Z., Z. Lu, X. Wen, B. Otto-Bliesner, A. Timmermann and K. Cobb: Evolution and forcing mechanisms of El Niño over the past 21,000 years, *Nature*, 515, 550-553, 2014.
- Lu, Z., Z. Liu and J. Zhu: Abrupt intensification of ENSO forced by deglacial ice-sheet retreat in CCSM3, *Clim. Dyn.*, 46(5), 1877-1891, 2016.
- 35 Lu, Z. and Z. Liu: Orbital modulation of ENSO seasonal phase locking, *Clim. Dyn.*, 2017. **Revision under review.**
- Masson-Delmotte, V. et al.: In *Climate Change: The Physical Science Basis*, Contribution of Working Group I to the Fifth Assessment Report of the Intergovernmental Panel on Climate Change [eds Stocker, T. F. et al.], 383–464, Cambridge Univ. Press, 2013.

- Meehl, G., Teng, H. and Branstator, G.: Future changes of El Niño in two global climate models, *Clim. Dyn.*, 26, 549–566, 2006.
- Meehl, G.A., T.F. Stocker, W.D. Collins, P. Friedlingstein, A.T. Gaye, J.M. Gregory, A. Kitoh, R. Knutti, J.M. Murphy, A. Noda, S.C.B. Raper, I.G. Watterson, A.J. Weaver and Z.-C. Zhao: Global Climate Projections. In: *Climate Change 2007: The Physical Science Basis*. Contribution of Working Group I to the Fourth Assessment Report of the Intergovernmental Panel on Climate Change [Solomon, S., D. Qin, M. Manning, Z. Chen, M. Marquis, K.B. Averyt, M. Tignor and H.L. Miller (eds.)], Cambridge University Press, Cambridge, United Kingdom and New York, NY, USA, 2007.
- Moy, C. M., G. O. Seltzer, D. T. Rodbell and D. M. Anderson: Variability of El Niño/Southern Oscillation activity at millennial timescales during the Holocene epoch, *Nature*, 420, 162–165, 2002.
- 10 Nakamura, H.: Midwinter suppression of baroclinic wave activity in the Pacific, *J. Atmos. Sci.*, 49, 1629–1642, 1992.
- Nakamura, H., T. Izumi and T. Sampe: Interannual and decadal modulations recently observed in the Pacific storm track activity and East Asian winter monsoon, *J. Clim.*, 15, 1855–1874, 2002.
- Neelin, J. D. and Co-Authors: ENSO theory, *J. Geophys. Res.*, 103, 14, 262–14, 290, 1998.
- Neelin, J. D., Jin, F. F. and Syu, H. H.: Variations in ENSO Phase Locking\*, *J. Clim.*, 13(14), 2570–2590, 2000.
- 15 Otto-Bliesner, B. L., E. C. Brady, G. Clauzet, R. Tomas, S. Levis and Z. Kothavala: Last glacial maximum and Holocene climate in CCSM3, *J. Clim.*, 19, 2006.
- Peltier, W.: Global glacial isostasy and the surface of the ice-age Earth: The ICE-5G (VM2) model and GRACE, *Annu. Rev. Earth Planet. Sci.*, 32, 111–149, 2004.
- Petit, J. R., Jouzel, J., Raynaud, D., Barkov, N. I., Barnola, J. M., Basile, I. and Stievenard, M.: Climate and atmospheric history of the past 420,000 years from the Vostok ice core, Antarctica, *Nature*, 399(6735), 429–436, 1999.
- 20 Philander, S. G.: *El Niño, La Niña and the Southern Oscillation*, Academic Press, London, 289 pp, 1990.
- Philander, S. G. and Fedorov, A.: Is El Niño sporadic or cyclic?, *Annual Review of Earth and Planetary Sciences*, 31, 579–594, 2003.
- Riedinger, M. A., M. Steinitz-Kannan, W. M. Last and M. Brenner: A ~ 6100 <sup>14</sup>C yr record of El Niño activity from the Galápagos Islands, *Journal of Paleolimnology*, 27, 1–7, 2002.
- 25 Roberts, W.: *An Investigation into the Causes for the Reduction in the Variability of the El Niño-Southern Oscillation in the Early Holocene in a Global Climate Model*, PhD thesis, Univ. Washington, 2007.
- Roberts, W. H., D. S. Battisti and A. W. Tudhope: ENSO in the mid-Holocene according to CSM and HadCM3, *J. Clim.*, 27, 1223–1242, 2014.
- 30 Russell, J.M. et al.: Glacial forcing of central Indonesian hydroclimate since 60,000 year BP, *Proc. Natl. Acad. Sci.*, 111:5100–5105, 2014.
- Stuecker, M. F., Timmermann, A., Jin, F. F., McGregor, S. and Ren, H. L.: A combination mode of the annual cycle and the El Niño/Southern Oscillation, *Nat. Geosci.*, 6(7), 540–544, 2013.
- Suarez, M. J. and Schopf, P. S.: A delayed action oscillator for ENSO, *J. Atmos. Sci.*, 45, 3283–3287, 1988.
- 35 Thomas, E., S.C. Clemens, Y. Sun, Y. Huang, W. Prell, G. Chen, Z. Liu and S. Loomis, Mid-latitude land surface temperature impacts the timing and structure of glacial cycles, *Geophys. Res. Lett.*, 44(2), 984–992, 2017.
- Thompson, C. and D. Battisti: A linear stochastic dynamical model of ENSO. Part I: Model development, *J. Clim.*, 13, 2818–2832, 2001a.
- 40 Thompson, C., and D. Battisti: A linear stochastic dynamical model of ENSO. Part II: Analysis, *J. Clim.*, 14, 445–466, 2001b.

- Timm, O., and Timmermann, A.: Simulation of the Last 21 000 Years Using Accelerated Transient Boundary Conditions\*, *J. Clim.*, 20(17), 4377-4401, 2007.
- Timmermann, A., F. Justino, F.-F. Jin, U. Krebs and H. Goosse: Surface temperature control in the North and tropical Pacific during the last glacial maximum, *Clim. Dyn.*, 23, 353-370, 2004.
- 5 Timmermann, A., S. Lorenz, S. An, A. Clement and S. Xie: The effect of orbital forcing on the mean climate and variability of the tropical Pacific, *J. Clim.*, 20, 4147-4159, 2007.
- Tudhope, A. W. and Coauthors: Variability in the El Niño-Southern Oscillation through a glacial-interglacial cycle, *Science*, 291, 1511-1517, 2001.
- Vimont, D. J., D. S. Battisti and A. C. Hirst: Footprinting: A seasonal connection between the tropics and mid-latitudes, *Geophys. Res. Lett.*, 28, 3923-3926, 2001.
- 10 Vimont, D. J., Wallace, J. M. and Battisti, D. S.: The seasonal footprinting mechanism in the Pacific: implications for ENSO\*, *J. Clim.*, 16(16), 2668-2675, 2003.
- Wang, C., Deser, C., Yu, J. Y., DiNezio, P. and Clement, A.: El Niño and southern oscillation (ENSO): a review, *Coral Reefs of the Eastern Pacific*, 3-19, 2012.
- 15 Waelbroeck, C., Labeyrie, L., Michel, E., Duplessy, J. C., McManus, J. F., Lambeck, K. and Labracherie, M.: Sea-level and deep water temperature changes derived from benthic foraminifera isotopic records, *Quat. Sci. Rev.*, 21(1), 295-305, 2002.
- Wittenberg, A. T.: Low-frequency variations of ENSO, *U.S. CLIVAR Variations*, 13(1), 26-31, 2015.
- Yeager, S. G., C. A. Shields, W. G. Large and J. J. Hack: The low-resolution CCSM3, *J. Clim.*, 19, 2006.
- 20 Yu, J.-Y. and Kao, H.-Y.: Decadal Changes of ENSO Persistence Barrier in SST and Ocean Heat Content Indices: 1958-2001, *J. Geophys. Res.*, 112, D13106, doi:10.1029/2006JD007654, 2007.

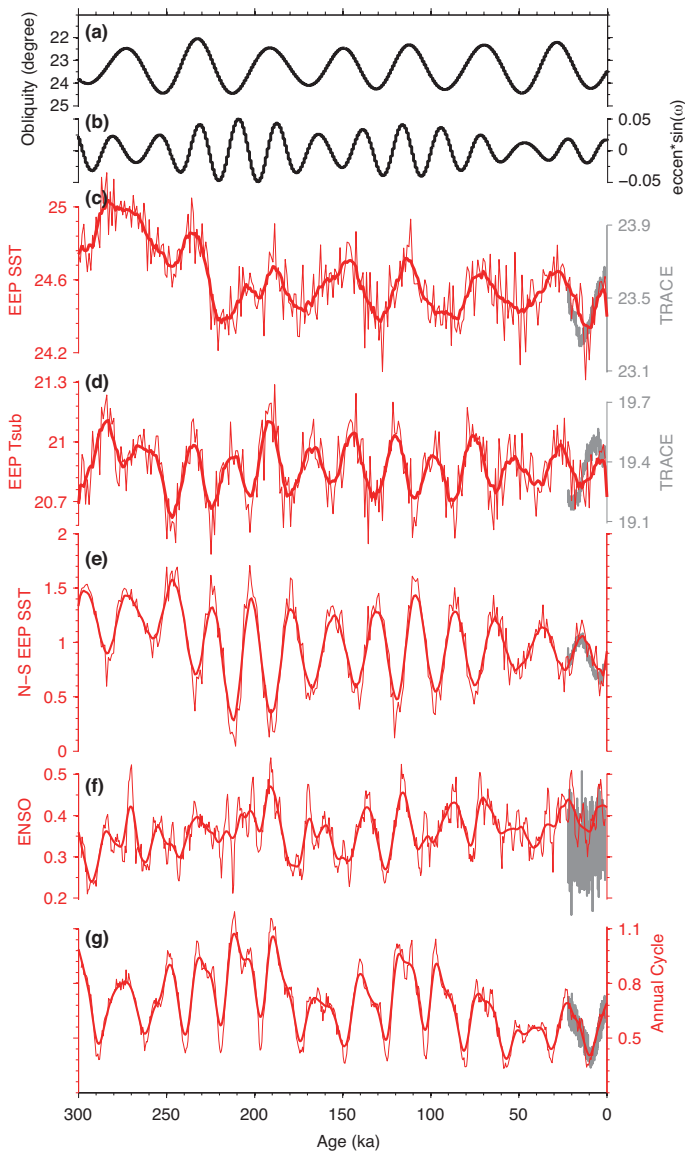
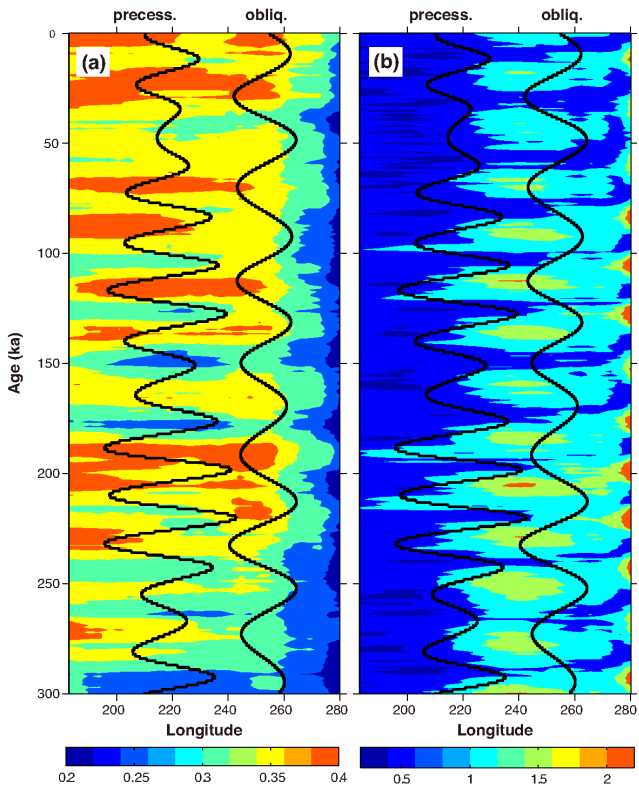


**Figure 1: Temporal evolution in the ORB simulation. Orbital forcing parameters (black color): (a) obliquity, (b) precession (sin of longitude of perihelion) modulated by eccentricity, defined as the precession index; Model output (red color): (c) eastern equatorial Pacific (EEP, 180W-80W, 5S-5N) decadal mean SST (thin line in 10-year windows, with thick line for 100-year running-mean smoothing), (d) EEP subsurface sea temperature (56m) (red dashed line) in 10-year windows with 100-year running-mean smoothing (e) N minus S SST of EEP (240E~270E, 10N-0 minus 10S-0, thin line in 10 year-windows, with thick line for 100-year running-mean smoothing) (f) ENSO variability, defined as Nino3.4 SSTA 1.5-7 year band-pass standard deviation in 30-year sliding windows (thin line with forward step of 5-year, thick line is for additional 100-year running-mean smoothing), (g) Nino3.4 SST annual cycle amplitude, defined as standard deviation of SST seasonal cycle in 30-year sliding windows (thin line with forward step of 5 years, thick line is for additional 100-year running-mean smoothing). Grey curves in (c)-(g) are the same variables from unaccelerated 21 ka TRACE-ORB simulation. In this study, calendar effect is not obvious. Also note that the acceleration technique is applied, for clarity, 'year' in all figure captions means model year.**



5 **Figure 2:** Evolution of the amplitudes (standard deviation in 10-year windows) of (a) interannual (1.5–7 years) variability and (b) annual cycle amplitude along the equatorial Pacific (5S–5N) in ORB. Note that interannual variability in (a) was further smoothed through 50-year running mean to filter out intra-model ENSO variability. The overlay curves represent orbital parameters of precession (modulated by eccentricity) (left) and obliquity (right), respectively.

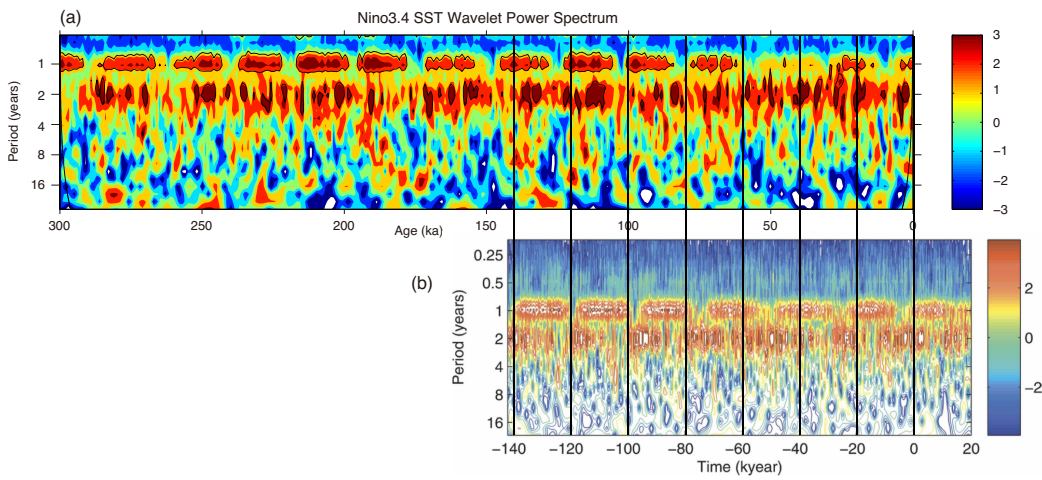
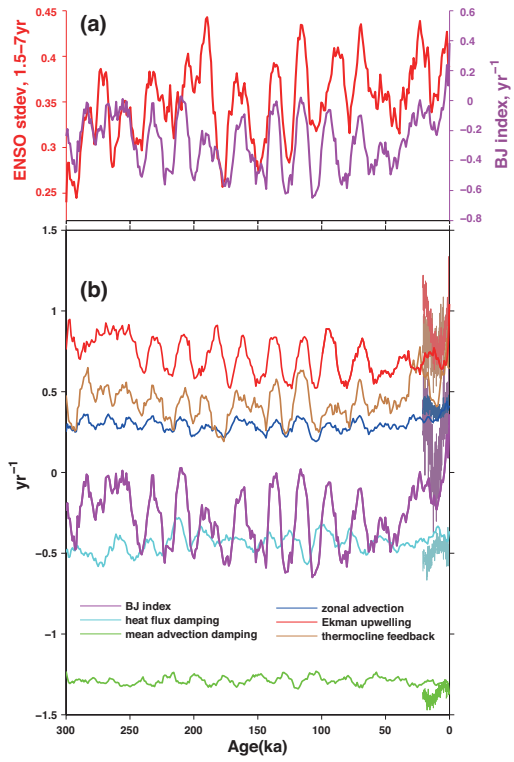


**Figure 3:** (a) Nino3.4 SST wavelet power spectrum in ORB. Black contour indicates a confidence level of 90%; (b) Nino3 SST wavelet power spectrum from Timmermann et al. (2007) Fig. 2. Vertical black lines at every 20 ka are used for aligning.



5 **Figure 4: Temporal evolution in the ORB simulation (in 30-year windows and with 300-year running mean smoothing). (a) ENSO variability (red) and BJ index (purple); (b) BJ index (purple) and its individual terms. Be noted that in (b) the Ekman upwelling feedback (red) and thermocline feedback (brown) have the largest signals in variability and dominate the trend of BJ index. Darkened curves in (b) are the evolutions of the same feedbacks calculated from unaccelerated 21 ka TRACE-ORB simulation.**

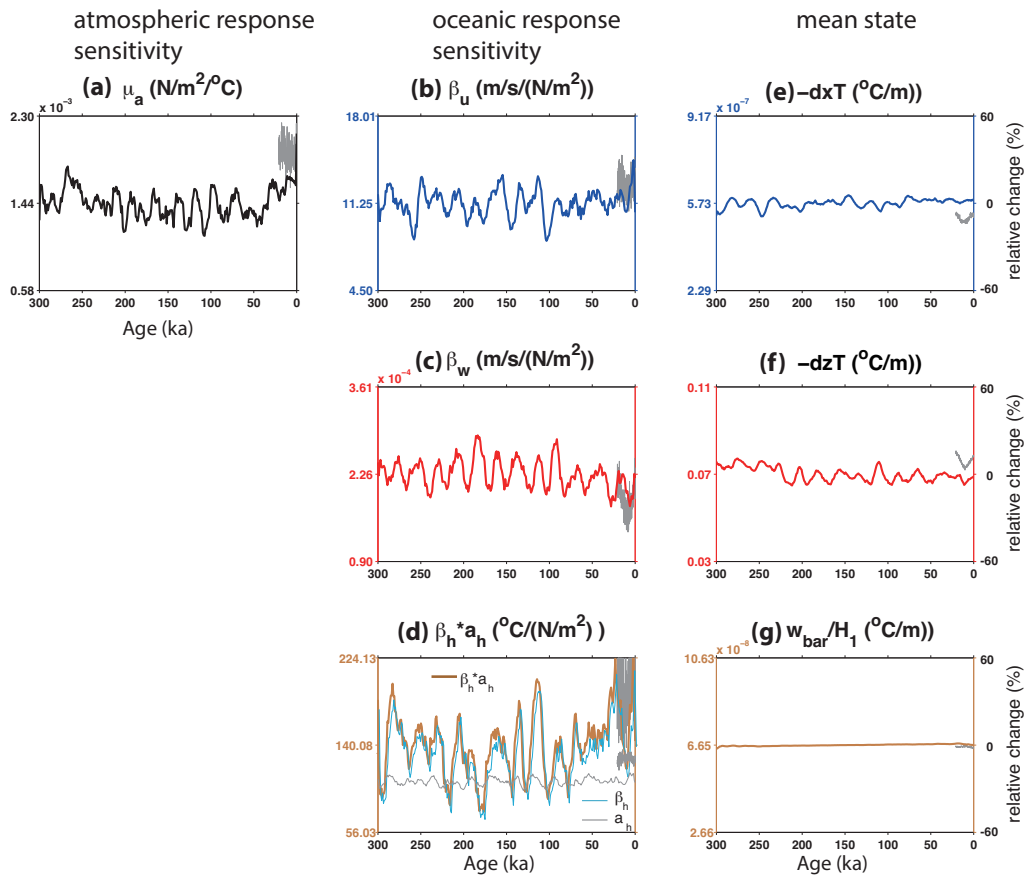
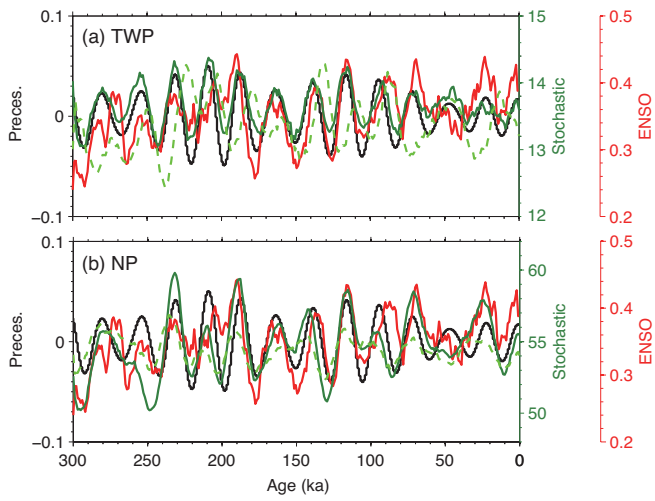
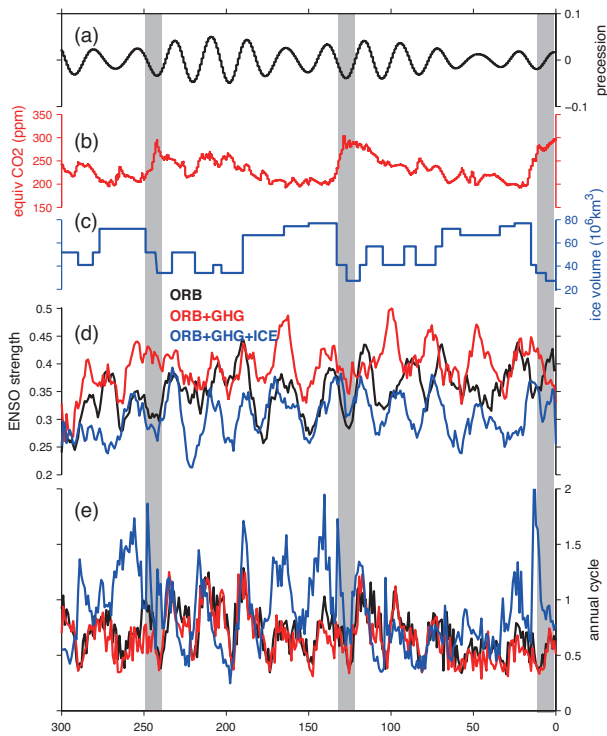


Figure 5: Components of BJ terms (in 30-year windows and with 300-year running mean). Left and middle panels are for regression coefficients, right panel is for mean states. Grey curves in each panel are the same variables calculated from unaccelerated 21 ka TRACE-ORB simulation.



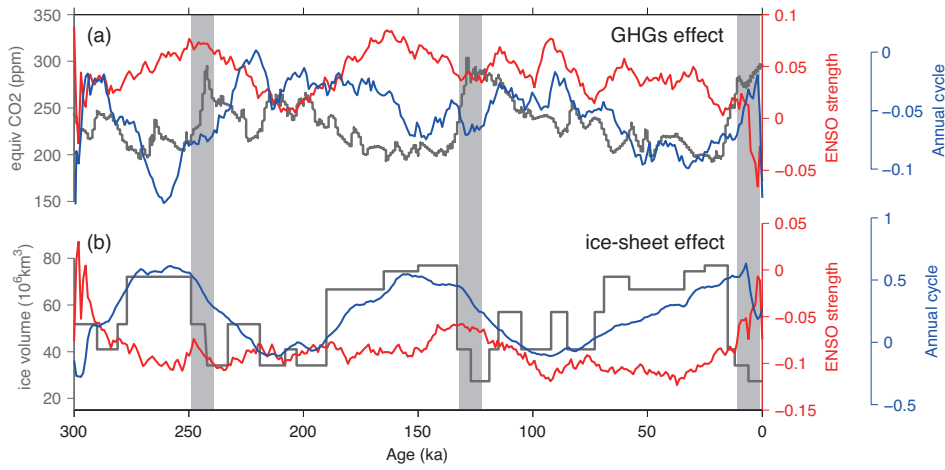
**Figure 6: Temporal evolution precessional forcing (black), ENSO variability (red), atmospheric noises over (a) tropical western Pacific and (b) North Pacific during intrinsic ENSO growth season AMJJAS (green, solid) and the whole year (green, dashed, vertically shifted to align with solid line). All except the forcing are in 30-year windows and with 300-year running mean smoothing.**

5



**Figure 7: Forcings: (a) precession index, (b) equivalent CO2 level, (c) global ice sheet volume; (d) ENSO variability and (e) annual cycle amplitude (derived using the same method as in Fig. 1f,g) for ORB (black), ORB+GHG (red) and ORB+GHG+ICE (blue). (d) and (e) are calculated in 30-year windows and with 300-year running mean smoothing. Vertical bars represent the full interglacial.**

10



5 **Figure 8: Temporal evolution of external forcing, ENSO variability and annual cycle amplitude. (a) the GHGs forcing effect: equivalent CO2 level (grey) and the GHGs effect on ENSO strength (red, using ENSO in ORB+GHG minus ENSO in ORB in Fig. 7d to indicate the pure GHGs effect) and annual cycle amplitude (blue, using annual cycle in ORB+GHG minus annual cycle in ORB in Fig. 7e); (b) the continental ice-sheet forcing effect: global ice sheet volume (grey) and the ice-sheet effect on ENSO strength (red, using ENSO in ORB+GHG+ICE minus ENSO in ORB+GHG in Fig. 7d to indicate the pure ice-sheet effect) and annual cycle amplitude (blue, using annual cycle in ORB+GHG+ICE minus annual cycle in ORB+GHG in Fig. 7e). All ENSO and annual cycle curves are smoothed by 400-year running mean. Vertical bars represent the full interglacial.**

1 Evolution and forcing mechanisms of ENSO over the last  
2 300,000 years in CCSM3

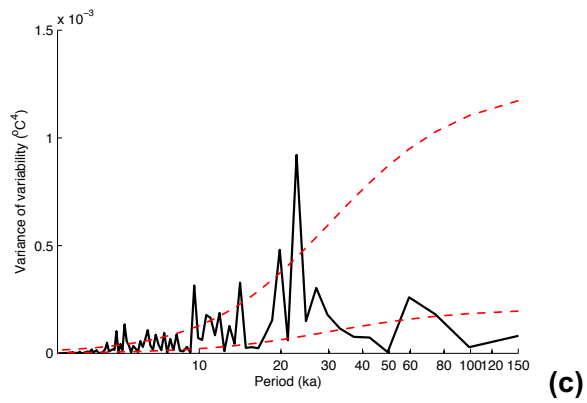
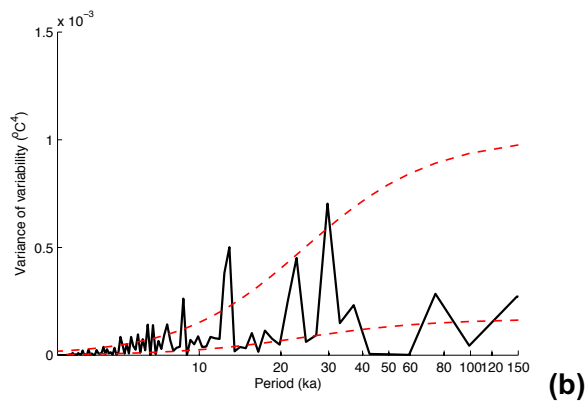
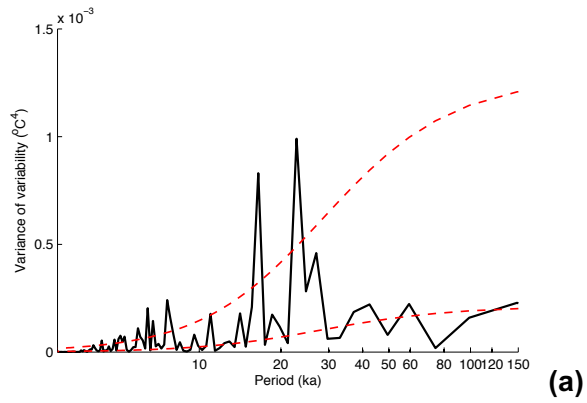
3 **Supplementary materials**  
4

5 Zhengyao Lu<sup>1\*</sup>, Zhengyu Liu<sup>2,1</sup>, Guangshan Chen<sup>2</sup> and Jian Guan<sup>1</sup>

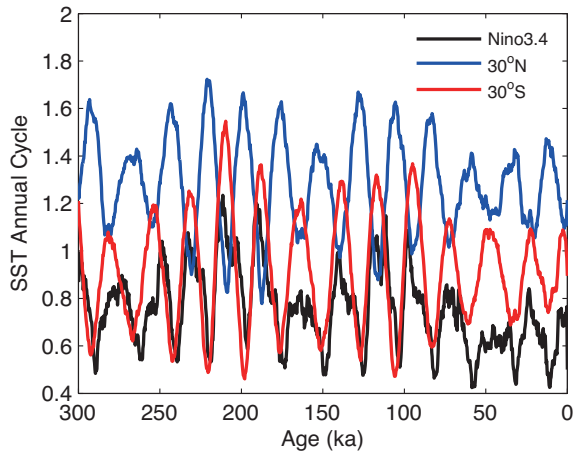
6 *1. Lab. Climate, Ocean and Atmosphere Studies, School of Physics, Peking Univ., Beijing, 100871, P. R. China*

7 *2. Dept. Atmospheric and Oceanic Sciences & Nelson Center for Climatic Research, Univ. of Wisconsin-Madison,*  
8 *Madison, WI53706, USA*

9  
10 \* Corresponding Author: Zhengyao Lu, Lab. Climate, Ocean and Atmosphere Studies, School of  
11 Physics, Peking Univ., Beijing, 100871, P. R. China,  
12 Email: zlu@pku.edu.cn; luzhengyao88@gmail.com



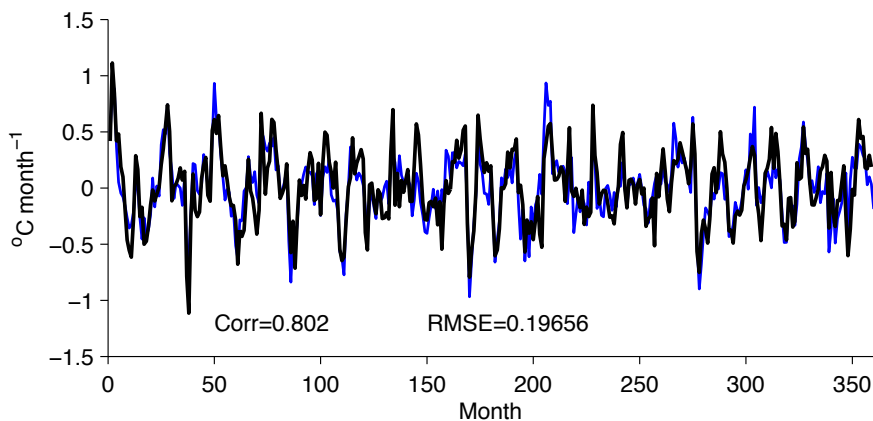
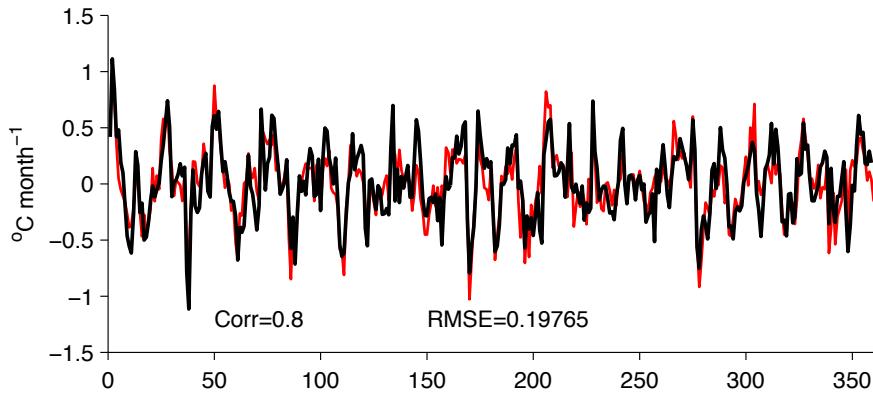
16 **Fig. S1** Power Spectra of ENSO variability for (a) ORB, (b) ORB+GHG and (c)  
 17 ORB+GHG+ICE. The red dashed lines show the power spectra of their corresponding red  
 18 noise and the 95% significance level.



19

20 **Fig. S2** Nino3.4 (black), 30°N (with longitude extent as Nino 3.4, blue) and 30°S (with  
 21 longitude extent as Nino 3.4, red) SST annual cycle amplitude in 30-year sliding windows  
 22 ( 5-year forward steps, with 100-year running-mean smoothing).

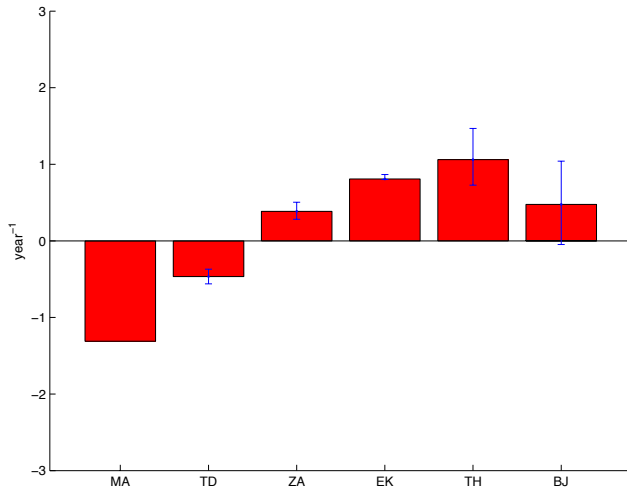
23



24

25 **Fig. S3** Last 30 model year of the mixed layer temperature tendency (black), anomalous heat  
 26 budget equation including only the linear terms (as those used to deprive the BJ index, red)  
 27 and both linear and nonlinear terms (blue). The correlation coefficient as well as the root  
 28 mean square error between the tendency and anomalous heat budget equations are shown in  
 29 the corresponding panel. Note that mixed layer depth is fixed.

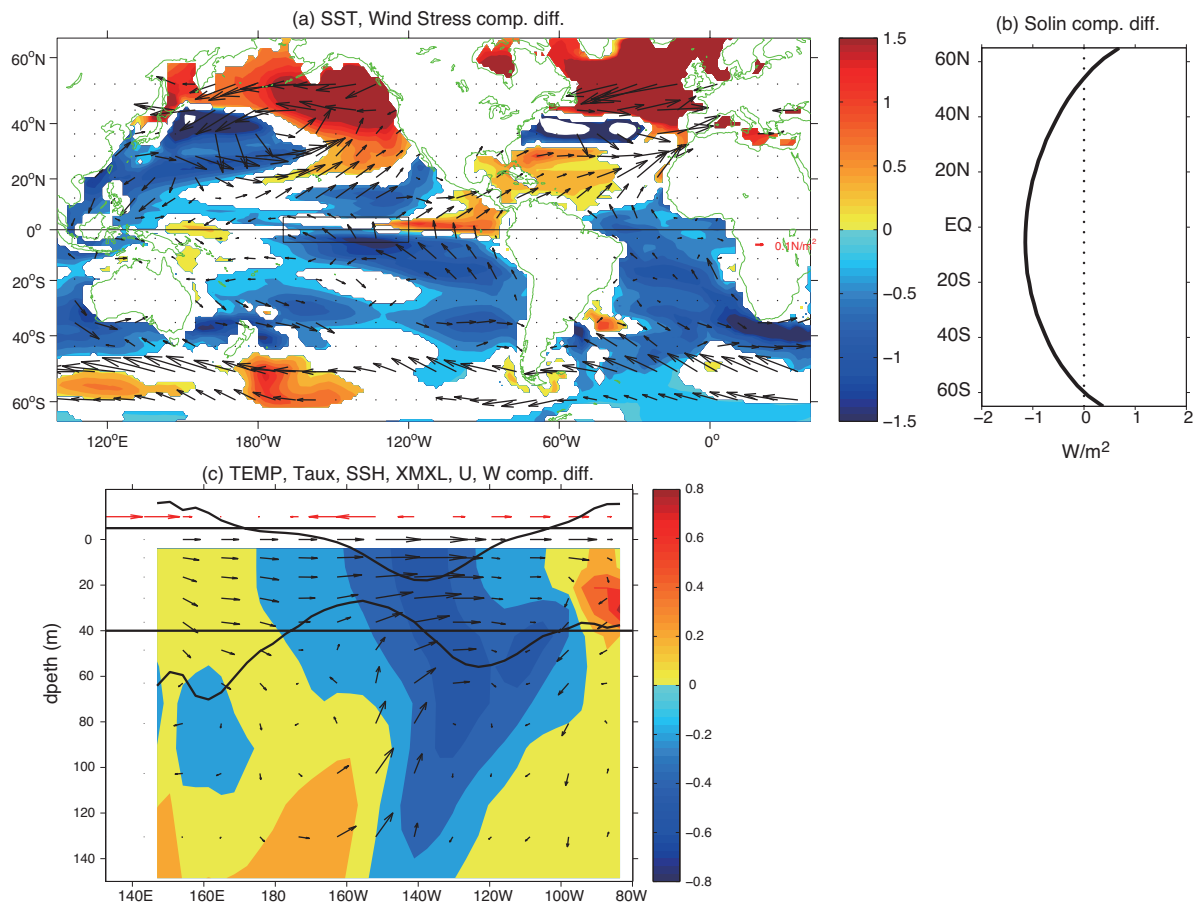
30



31

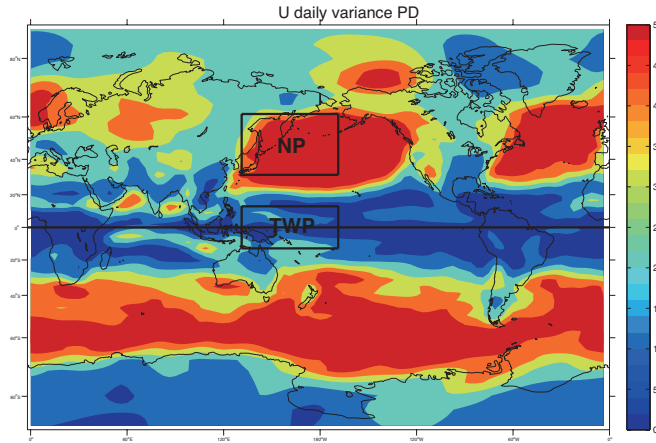
32 **Fig. S4** The BJ index and its contributing terms of the last 30 model years. Error bars estimate  
 33 the error from regression.

34



35

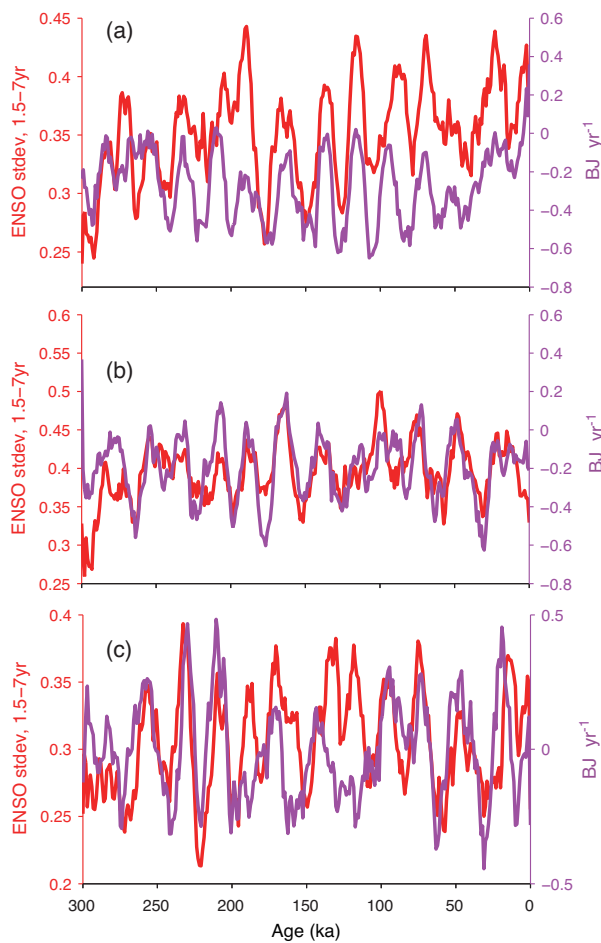
36 **Fig. S5** Composite mean state difference (low precession minus high precession). (Upper  
 37 panel) SST (shading), surface tau (vectors) and zonal mean insolation; (lower panel) cross  
 38 section of sea temperature (shading), ocean current (black vectors), surface tau (red vectors),  
 39 SSH (upper black curve) and mixed layer depth (lower black curve, using model output  
 40 XMXL).



41

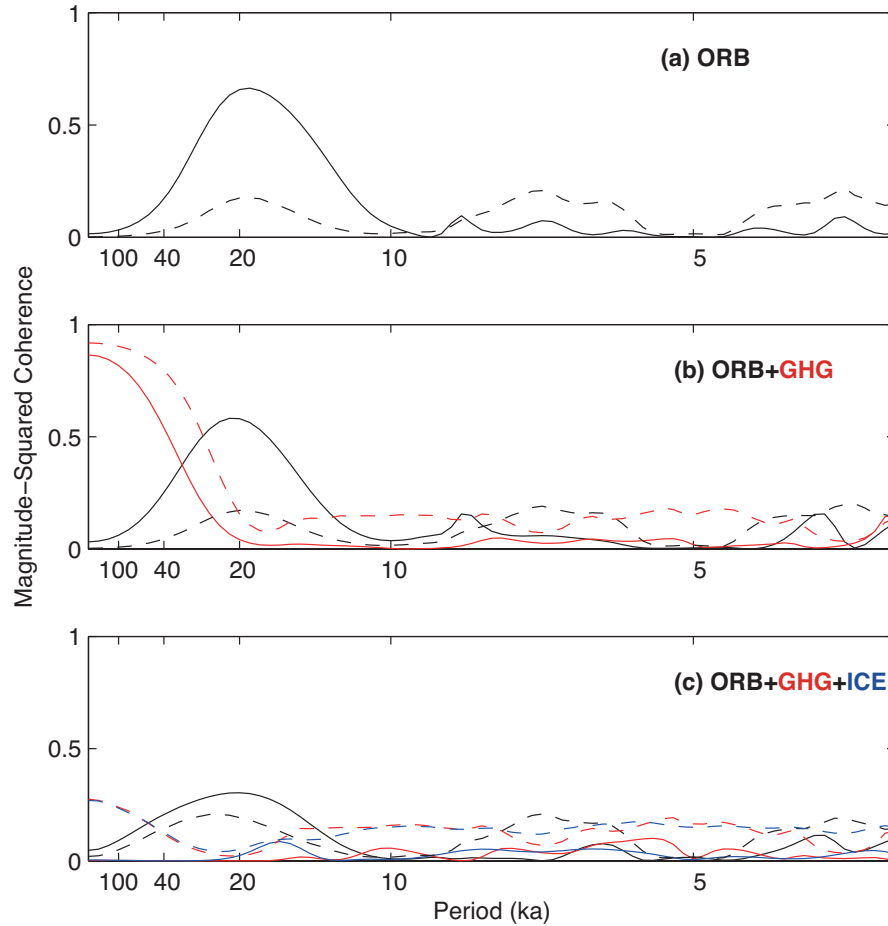
42 **Fig. S6** Distribution of monthly mean variance of daily surface U wind (derived from  
 43 monthly U and UU) in ORB (present day), and the black boxes depict the tropical western  
 44 Pacific (15S–15N, 120–190E) and North Pacific region (30N–60N, 130E–190E) when plotting  
 45 Fig. 7.

46



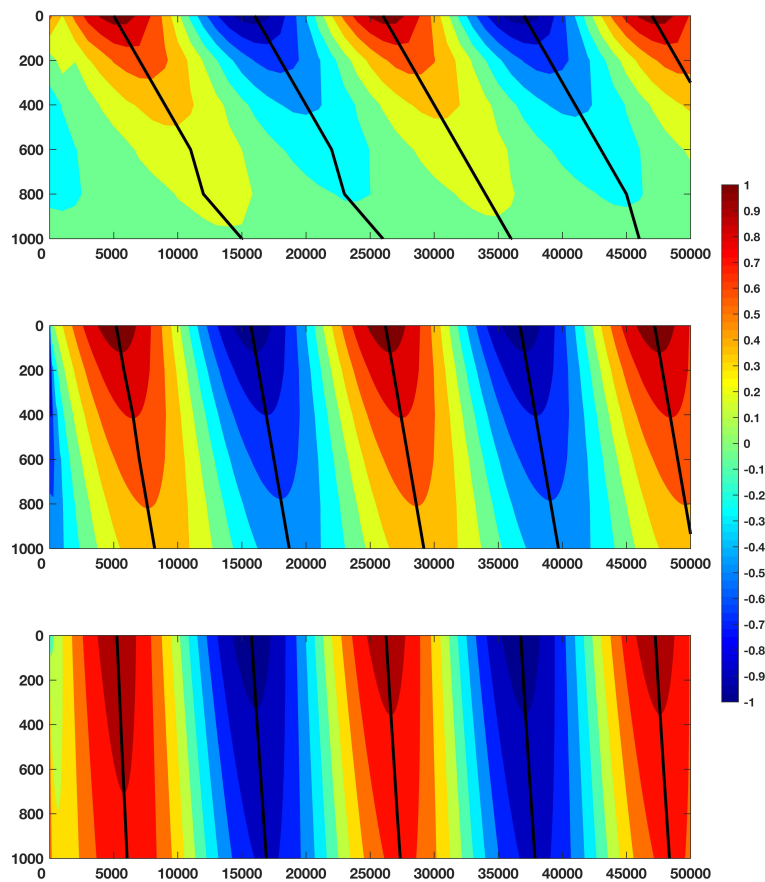
47

48 **Fig. S7** Temporal evolution of ENSO (red) variability and BJ index (purple) (in 30-year  
 49 windows and with 300-year running mean smoothing) for (a) ORB simulation; (b)  
 50 ORB+GHG simulation and (c) ORB+GHG+ICE simulation.



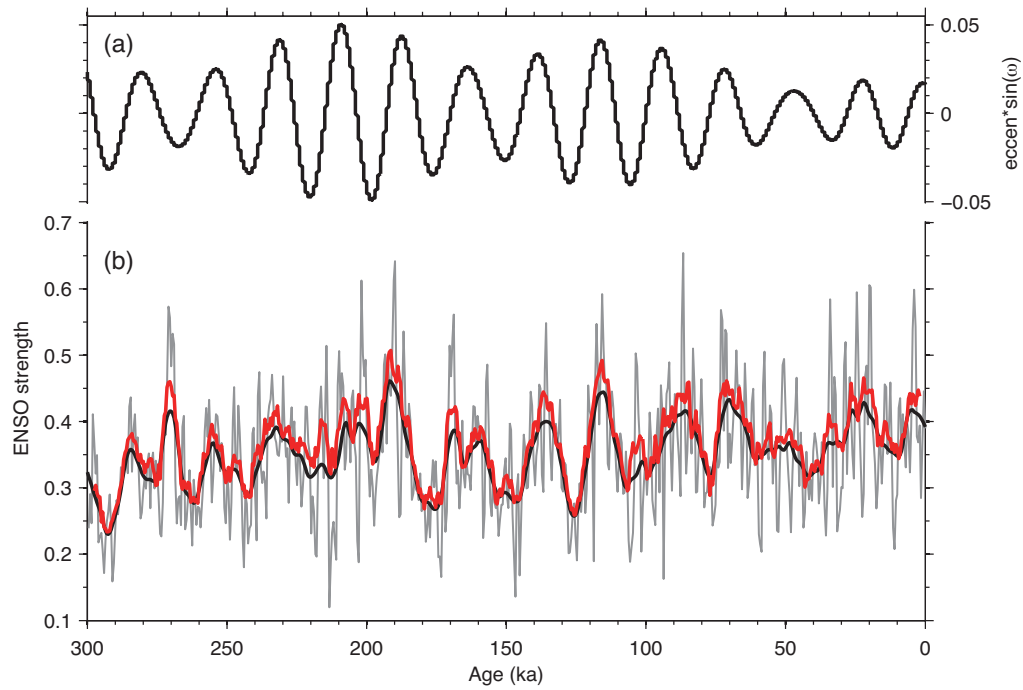
51

52 **Fig. S8** Coherence of BJ index and external forcing. The solid curves are coherence of BJ and  
 53 precessional forcing (black), GHGs forcing (red) and ice-sheet forcing (blue), respectively.  
 54 The dashed curves are 95% significant level (derived by resampling of one time series  
 55 without replacement 1000 times and calculate coherence distribution for the uncorrelated  
 56 series), with the corresponding color to each forcing. (a) ORB simulation; (b) ORB+GHG  
 57 simulation and (c) ORB+GHG+ICE simulation.



58

59 **Fig. S9** Time sequence of the vertical temperature profile in a simple diffusion model under  
 60 three acceleration scenarios: (upper panel) 100-fold acceleration, (middle panel) 10-fold  
 61 acceleration and (bottom panel) non-acceleration. Y-axis is depth (m) and x-axis is  
 62 accelerated year, and the contour is the anomalous temperature ( $^{\circ}\text{C}$ ). Black lines connect the  
 63 maximum signals in the ocean. The x-axis time scale of upper and middle panels is stretched  
 64 by a factor of 100 and 10 to illustrate the phase shift in the deep ocean.



65

66 **Fig. S10** Test the robustness of orbital scale trend in ENSO variability. (a) the precession  
 67 index; (b) Nino3.4 SST 1.5-7 year band interannual variability in 10-year sliding windows  
 68 and 5-year forward step (grey curve) with additional 100-year running-mean smoothing  
 69 (black curve), and in 50-year sliding windows and 5-year forward step (red curve). Note that  
 70 the aforementioned 'year' is model year.